Summer 2013

Direct - drive permanent magnet synchronous generator design for hydrokinetic energy extraction

Amshumaan Raghunatha Kashyap

Department:

DIRECT - DRIVE PERMANENT MAGNET SYNCHRONOUS GENERATOR DESIGN FOR HYDROKINETIC ENERGY EXTRACTION

by

AMSHUMAAN RAGHUNATHA KASHYAP

A THESIS

Presented to the Faculty of the Graduate School of the

MISSOURI UNIVERSITY OF SCIENCE AND TECHNOLOGY

In Partial Fulfillment of the Requirements for the Degree

MASTER OF SCIENCE IN ELECTRICAL ENGINEERING

2013

Approved by

Dr. Jonathan W Kimball, Advisor
Dr. Mehdi Ferdowsi
Dr. K Chandrashekhara

ABSTRACT

Hydrokinetic turbines deliver lower shaft speeds when compared to both steam and wind turbines. Hence, a water wheel generator must operate at speeds as low as 150 – 600 rpm. This thesis describes a permanent magnet synchronous generator (PMSG) that was designed, built, and tested to serve a low speed hydrokinetic turbine. The design methodology was emphasized since designing an application specific generator poses various design and hardware construction issues. These are torque, speed, power and start-up requirements. This generator was built to operate without a speed increaser, implying very low speeds. FEA and performance results from the simulation done in ANSYS - RMXprt® and Maxwell® 2D respectively are presented. The hardware test results demonstrate that the generator performs satisfactorily while reducing the cogging torque to the greatest possible extent.

ACKNOWLEDGEMENTS

I would like to express my deepest appreciation and my highest regards to my research advisor and committee chair, Dr. Jonathan W. Kimball. His knowledge and expertise are second to none and, with his enthusiastic, energetic charisma, he has served as a role model to me throughout my graduate studies. I am very thankful to the invaluable knowledge and sense of discipline he has ingrained in me. More over to the generous financial support he has provided me all throughout, in the form of research assistantship. This thesis would not have been possible without his guidance and help.

I would also like to thank my thesis committee members, Dr. Mehdi Ferdowsi and Dr. K. Chandrashekhara, for their help and guidance. Their appreciation and support has been a consistent source of encouragement. I also extend my gratitude to my colleagues on the mechanical team who helped me better understand the mechanical aspects of this project.

I would like to make a special mention of Mr. Gregory Taylor for his crucial help with the generator's drawings and 3D models. I want to thank all of my lab mates for their constant support, both personally and professionally. I deeply appreciated the interest in my project they always seemed to convey.

I could not have accomplished any of this work without my parents care and support. Their motivation and sacrifice for my well-being has been immense. I express my deepest gratitude to them from the bottom of my heart.

Finally, I would like to gratefully acknowledge the support of the Office of Naval Research through contract ONR N000141010923 (Program Manager - Dr. Michele Anderson). Their financial support made my research possible.

TABLE OF CONTENTS

Page

LIST OF ILLUSTRATIONS

Page

LIST OF TABLES

Page

NOMENCLATURE

WECS	Wind Energy Conversion System
DFIG	Doubly Fed Induction Generator
BLDC	Brushless DC machine
PMSG	Permanent Magnet Synchronous Generator
TWh/yr	Terra Watt hour per year
MWh	Mega Watt Hour
KWh	Kilo Watt Hour
MW	Mega Watt
kW	Kilo Watt
GW	Giga Watt
NYSERDA	New York State Energy Research & Development Authority
CVT	Continuously Variable Transmissions
rpm	Rotations per minute
P_{gear}	Power lost in the gearbox
P_{gearm}	Percentage loss in gearbox at rated speed
N	Rated speed of rotation in rpm
N_{actual}	Current/Actual speed of rotation in rpm
f	Frequency of rotation of synchronous field
P	Number of Poles
L_m	Axial length of each magnet
ϕ_g	Magnetic flux
B_{av}	Average Flux density
D	Stator inner diameter
L	Length of stator
N_s	Number of stator slots

N_{spp}	Number of slots per pole per phase
N_m	Number of slots per magnet pole
N_{ph}	Number of phases
T_e	Electrical torque
B_m	Friction constant
ω_{rm}	Rotor mechanical speed
T_L	Load torque
J	Total inertia
τ	Torque generated due to inertia
I	Moment of inertia
α	Angular acceleration
M	Mass of the body
r	Radius of disc from center
L_m	Length of magnet
θ_P	Pole pitch angle
τ_P	Pole pitch
S_e	Extra arc length considering 90% of magnet occupying rotor
M_{ir}	Magnet inner radius
R_e	Calculated extra radius
T_{cog}	Cogging torque
R	Reluctance
θ	Rotor position
ω_{bi}	Back iron
B_{max}	Maximum allowed flux density
k_{st}	Stacking factor

t_s	Slot pitch
ω_{tb}	Tooth width
N_{sm}	Number of slots per magnet
μ_r	Relative permeability
σ	Electrical conductivity
H_c	Co-ercive force
$\vec{\tau}$	Torque vector
$\vec{F}$	Force vector
V_{ab}	A to B line – to – line voltage
V_{bc}	B to C line – to – line voltage
V_{an}	Phase A to neutral phase voltage
n_{st_lam}	Number of stator laminations
t_{lam}	Thickness of each lamination
k_f	Filling factor
n_{rt_lam}	Number of rotor laminations
L_{rot}	Length of rotor
n_s	Number of turns in each slot
e_{max}	Maximum back e.m.f produced
k_d	Distribution factor
k_p	Pitch factor
k_s	Skew factor
R_{ro}	Rotor outside radius
ω_m	Rotational speed in ‘rps’

rps	Rotations per second
V_{rms}	RMS voltage
I_{rms}	RMS current
n	Number of samples
P_{rms}	RMS power in one phase
G	Conductance
mph	Miles per hour

1. INTRODUCTION

1.1. INVESTING IN HYDROKINETICS

Renewable energy extraction techniques have gained momentum in the wake of depleting natural resources. Many developed and developing countries alike are currently focused on producing more renewable energy. This focus is supported by tremendous investments. This change is necessary to curb the effect of rise in oil prices globally. The European Union alone recorded a 9.9% dip in oil consumption in 2012 [1, 2]. This reduction was primarily due to increased renewable energy production. An elevated level of interest in renewable energy production around the globe has helped renewables compete against conventional oil resources. The global renewable energy share in the energy production market rose to 2.1% in 2012 as opposed to 0.7% in 2001. Hydrokinetic energy production from the US contributed a monstrous share of 9.4% of global renewable energy produce as of 2011. 3.3 % of energy produced in the US as of 2010 was from hydrokinetics as well [1, 2].

As observed from the recent trends in other major contributors like China, Brazil, India and Canada, developing better technologies for hydrokinetic energy extraction offers promising returns [3, 4].

1.2. COMPARISON BETWEEN INDUCTION MACHINE AND PERMANENT MAGNET SYNCHRONOUS GENERATOR

A wind energy conversion system (WECS) has the greatest potential thus far as a renewable energy resource. Many techniques have been developed for hydrokinetics based on the principle of WECS. It is because from an energy conversion point of view,

both WECS and hydrokinetics share the same logic for conversion. Any technical breakthrough or improvement in electrical devices, mainly generators, can benefit both areas. The most common choices for hydrokinetic and wind turbines are the doubly fed induction generator (DFIG), squirrel cage induction generator (SCIG) and the permanent magnet synchronous generator (PMSG).

Induction generators are most commonly used in WECS because they offer the most rugged, cost effective solution as a conveniently mass produced machine [5-7]. The DFIG is also able to supply power at both a constant voltage and a constant frequency. Meanwhile the rotor speed varies, making this generator suitable for variable-speed wind and hydro-power generation [8]. It is normally used in high power systems to utilize these advantages. Similarly, variations of the PMSG can be used for both high and low power applications as appropriate [9-11].

It is essential to compare the two generators to make a unique choice. Thus efficiency and performance comparison between the induction machine and the PMSG has been shown in article [12].

Several effects must also be considered (i.e. voltage sags, stability issues and power losses) when selecting between DFIG and PMSG [13]. PMSGs are most commonly used for both small scale hydrokinetic and wind turbine applications, because of their high reliability, simple structure, low noise, and high power density.

1.3. STUDY OF RELEVANT WIND AND HYDROKINETIC TURBINE TECHNOLOGY

This study maintains that technology and research considered for wind turbines holds true for hydrokinetic turbines as well. It is important to know the energy conversion methodology of both resources and thus understand why they are the same.

1.3.1. Working Principle of Hydrokinetics and WECS. Wind energy is typically described as a form of solar energy because heated air produces wind [14]. This wind energy can be utilized to generate electricity. A wind turbine can be imagined as operating the opposite way a table fan operates. Wind turbines are usually mounted atop a huge tower in potentially windy areas. Several elements like the gearbox, generator, controller and shafts go into this mounting. The most significant elements are the huge blades that turn when wind is blown over them. These rotor blades rotate the generator shaft and supply it with mechanical power. The shaft connected to the blades is a low speed shaft; the gearbox connects/converts it to high speed shaft. A typical blade speed shall be 30 – 60 rpm. The speed is then converted to 1000 – 1800 rpm or sometimes 3000 rpm with the help of suitable gear ratio inside the gearbox.

The high speed shaft is connected to the generator's rotor thus generating electricity. Other sensors such as the anemometer and the wind direction sensor feed the controller and help regulate the turbine's action. Both the yaw drive and the yaw motor continuously align the turbine blades in the wind's direction to generate maximum energy as seen in Figure 1.1.

High water head turbines (i.e both the Kaplan and the Francis turbines) generate electricity from the potential energy stored in the water heads. A hydrokinetic turbine, however generates from the kinetic energy present in flowing water. This effect of water

(fluid) on the blade thus impacts the blade's design The amount of force applied on the blade varies according to the element utilized: either air or water. Additional significant changes are primarily, mechanical [Referring to Figure 1.2] (i.e the coupling and the gearbox).

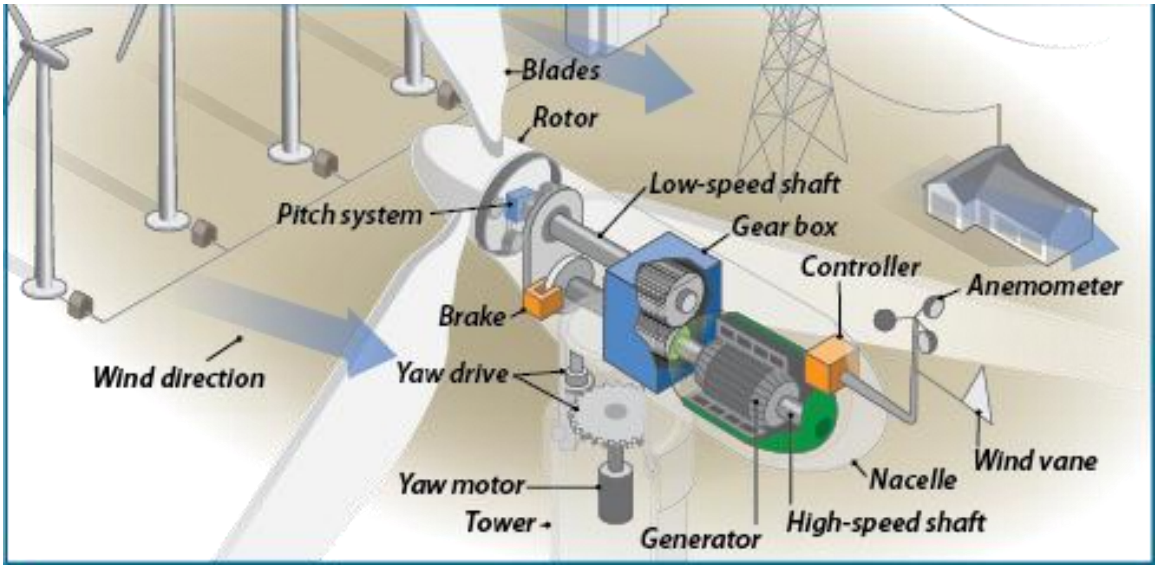

Figure 1.1: Various sections of a wind turbine

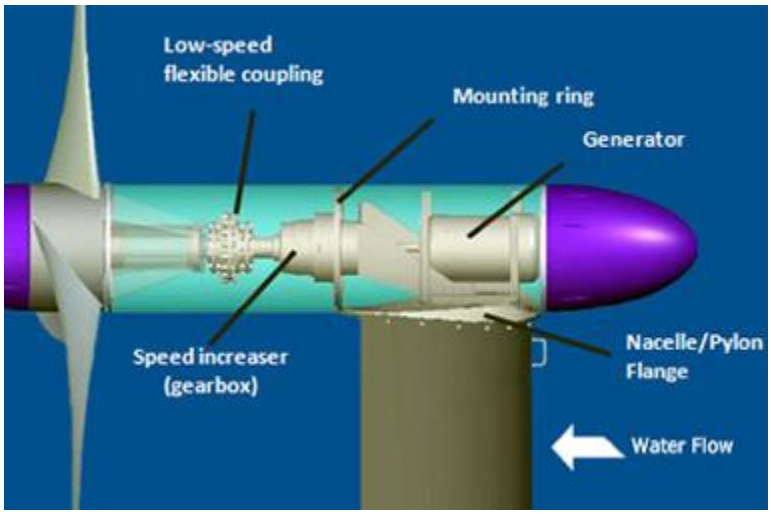

Figure 1.2: Various sections of a hydrokinetic turbine

Finally an anemometer is used for a wind turbine while water specific sensing equipment is used for hydrokinetic turbines. A mechanical rotor with a slow speed shaft converted to a high speed shaft runs into the generator for both wind and hydrokinetic turbines. The choice of both a generator and power regulation methods may be either situational or design-specific. The principle of operation for both turbines however remains the same.

Hence, energy conversion discussions that hold good for a wind turbine also holds equally good for hydrokinetic turbine too. Henceforth, this shall be taken advantage of in various sections and the hydrokinetic turbine system is treated like a wind turbine system.

1.3.2. Overview of Available Resources. The demand for renewable energy is projected to rise rapidly in the next decade. Thus identifying potential locations and deploying relavent technologies is key. Interestingly the US holds the second spot [15] behind the UK in both wave and tidal energy systems being explored, in the development stage or even available commercially. This section focusses on both tidal and wave energy conversion systems. Many factors, such as flow rate of water in the river bed, depth unto which the system can be immersed to, blockage ratio of the turbine system play an important role in deciding whether or not a particular region can house a hydrokinetic turbine. The ratio of technically recoverable power to theoretically available power for various configurations of hydrokinetic systems [16] provides a better, practical idea. The lower Mississipi region offers the highest technically recoverable annual energy with 57.4 TWh/yr followed by New York and Ohio.

Many additional states in the US house either rivers or sea beds that offer a great deal of opportunity for wave energy extraction. As a result the potential for wave energy,

tidal energy, and hydrokinetic energy production is much higher than that for any other type of renewable energy form in the US [17]. For example, in 2011 alone, 319,355 GWh of conventional hydroelectric power was produced as opposed to 120,177 GWh of wind energy systems. The problem with hydroelectric production is that it varies from year to year. This variation makes it difficult to estimate both productivity and contribution to total annual energy generation. Even with a tremendous magnitude of energy produced, hydroelectric production falls short by huge numbers when compared to coal, petroleum and nuclear energy production [18]. The advantage of tidal energy over these other resources is that tidal energy is free of cost. Whereas petroleum and coal products must be purchased and most often imported.

Washington state currently leads the way in hydroelectricity production with 77,636,758 MWh as of 2008. It is followed by Oregon and California, respectively [18]. River bed states, e.g., Missouri and Tenessee have also shown good numbers with regard to emerging technologies. Technology improvement is only one aspect of improving the market share for hydrokinetics. This new technology must also comply with numerous federal and environmental laws and regulations [19] to become a commercially licensed project. Sections of the law i.e., the "Jobs and Economic Development Impact (JEDI) model," the " Energy Policy Act (EPAct) of 2005," and the "MOU between State of California and FERC in 2010" [20], highly encourage innovative hydrokinetic projects, providing both fiunancial incentives and other forms of support.

Ultimately, a paradigm shift in hydroelectricity production can occur only if better, profitable and efficient topologies of hydrokinetic turbines are developed to utilize the available water resources found both in river and sea beds. The renewable energy market

certain;ly appears to be growing, as evidenced by the recent governmental hydrokinetic project license sanctions [21], and the Roosevelt project, the first ever tidal project sanctioned in the New York area in 2012. A few such projects are introduced in the following section.

1.3.3. Topologies of Wind and Hydrokinetic Turbines. Wind turbines can be classified into one of two very broad categories namely:

1. Horizontal axis turbines
2. Vertical axis turbines (Known as the Darrieus model)

The primary difference between these two turbines is the blade configuration. The turbine blades face the wind or rotate along the wind direction, respectively. The horizontal axis wind turbine is mounted on tall towers so that it can operate in either upstream or downstream wind directions. It produces larger amounts of electricity more efficiently than a vertical axis turbine produces. It does so because wind speeds are lower at ground levels; vertical axis turbines are used at higher altitudes. Additionally horizontal axis turbines can operate at a speed of 16 – 18 mph and a maximum speed of 55 mph. Above this speed, it experiences huge turbulences. Vertical axis turbines can handle much higher speeds, though they are rarely exposed to such. A horizontal axis is thus preferred because it can generate higher power at a lower investment with minimal maintenance (see Figure 1.3). Another important classification is based on both the type of generator and coupling used, as demonstrated in Figure 1.4. Additional factors by which a wind turbine can be classified are illutrated in Figure 1.5.

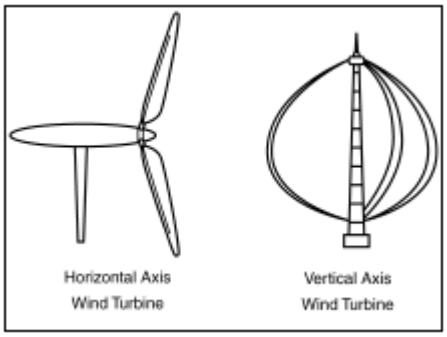

Figure 1.3: Structural comparison of horizontal and vertical axis turbine structures

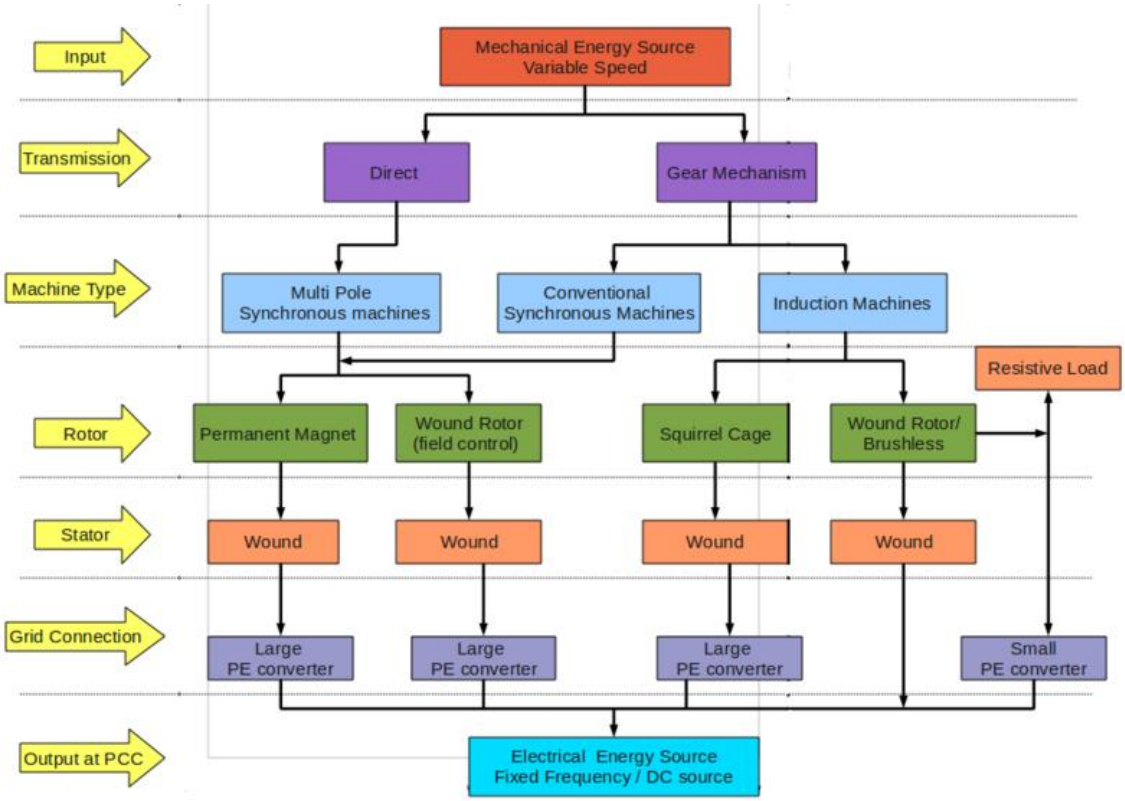

Figure 1.4: Classification of generators for wind turbines [22]

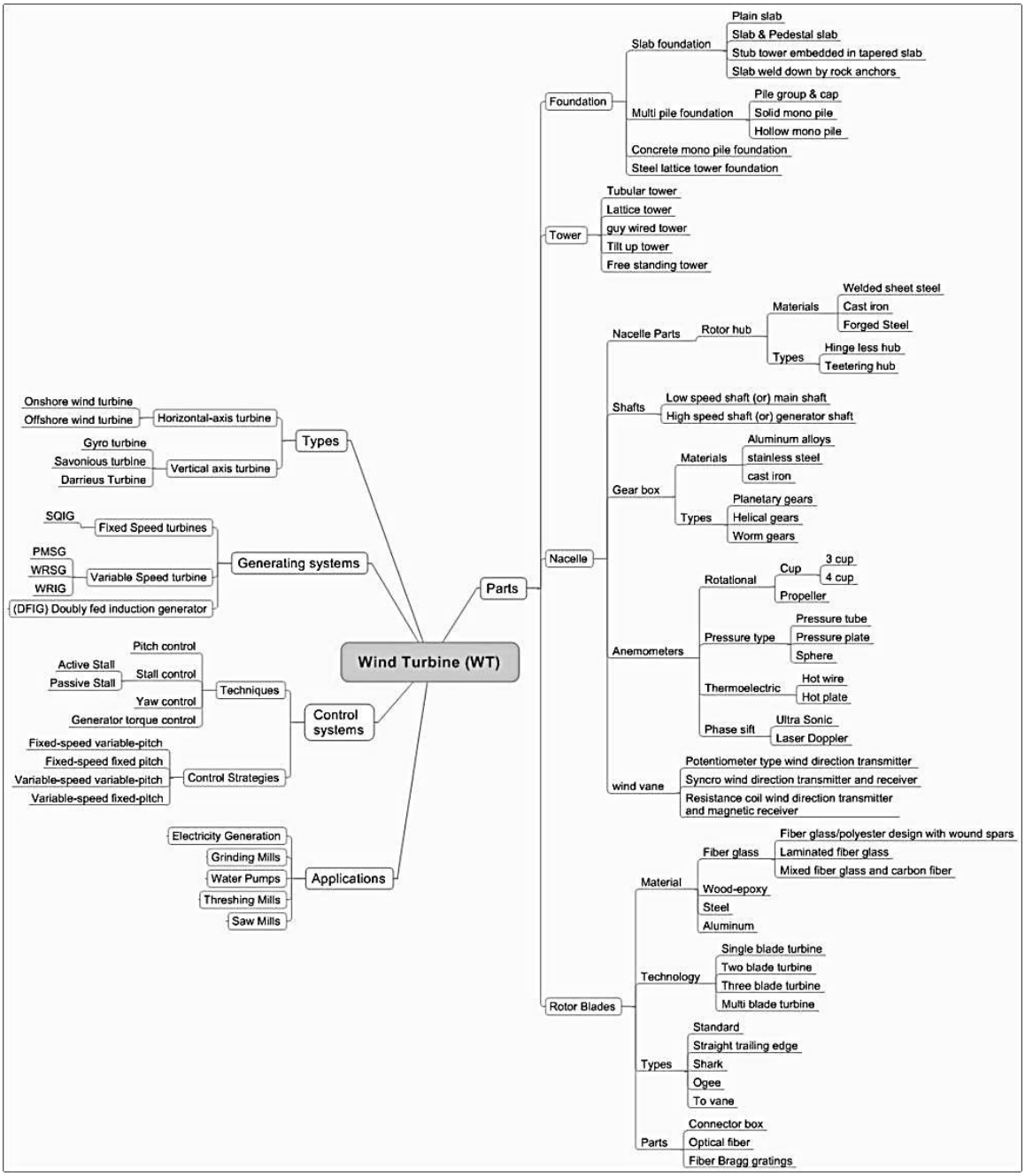

Figure 1.5: Broad classification of wind turbines

Hydrokinetic systems are classified according to how they harness the kinetic energy in water. These classifications include the following:

1. Wave Energy Conversion Systems (WECS) - Relies on high tides/waves. Further classified as:
    - Oscillating water column
    - Point absorber
    - Attenuator
    - Overtopping device
2. Rotating devices (tidal turbine) – Relies on a constant flow of water as in the rivers

These topologies are explored in the following section.

1.3.4. Wave Energy Conversion Topologies Explored. Recent studies have focused on both the modifications of and the new designs for Wave Energy Conversion topologies. Of these topologies, horizontal axis turbines have been widely explored. They are further classified into two-blade, three blade and multi-blade turbines. Many research projects are being conducted at the university level in many states.

At the Missouri University of Science and Technology, a horizontal axis tidal turbine is being researched [23] with composite material technology for the 3 blades. Multiset blade system and ducted structures are also being explored. This turbine is directly attached to the generator being developed in this article, making it a direct drive turbine system. Some of the similar WECS and tidal turbines are visualized in Figure 1.6. and explored further.

Figure 1.6: Sample of different configurations and concepts of hydrokinetic turbines explored at various institutions [15]

Figure 1.7 can be related to Section 1.3.1 to understand the rest of the energy conversion stage.

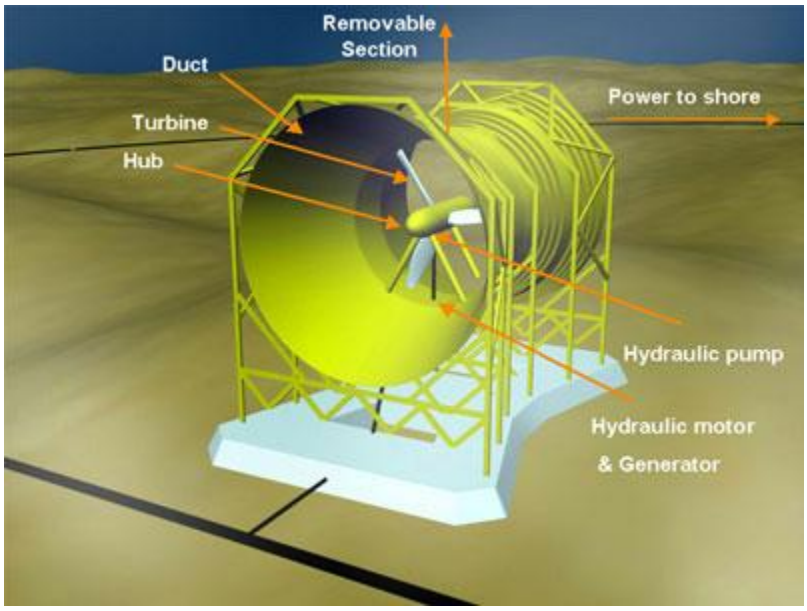

Figure 1.7: The hydrokinetic turbine model from the Lunar Energy project [24]

Many innovative designs in the horizontal axis turbine domain have been proposed and implemented [25, 26]. Each design interacts differently with the flow of water. The generation capabilities are between 100 kW and 1 MW. Although they are bulky, they are efficient. Their maintenance has been simplified to a great extent. Some of them are reviewed in the following section.

1.3.4.1 RITE Project from Verdant Power. Also known as the 'Free Flow' system, this project is a tidal energy extraction project located in the East River, NY [27]. The turbine system has a 3 blade horizontal axis turbine with a 5m rotor diameter and a passive yaw mechanism. The blades rotate with a slow but constant speed of 40 revolutions per minute (rpm), with tip speeds of $35\ \mathrm{ft/sec}$ well below conventional hydropower turbine blade speeds. The estimated hydropower energy production from this

venture is 100 – 500 MW. The turbine system has an efficiency of 38% to 44% with a water current speed of $7\ \mathrm{ft/sec}$ (1.8 to 4.2 knots). It connects to an underground low voltage cabling system, delivering its power to a short distance shore control room. The turbine system is now certified from FERC to be an emission-free, fully functional turbine with a license to operate.

More ventures from both Verdant Power and NYSERDA have been attached with this project in the East Channel of the East River in New York. Its prime purpose is to continue the demonstration of the technology for reliability, longevity, cost-effective O&M and environmental compatibility.

1.3.4.2 Lunar Energy (U.S – D.O.E). The system here has a multi-blade, tidal current, horizontal axis, hydrokinretic turbine system [24]. The system itself is known as the Rotate Tidal Turbine (RTT). The turbine has a duct around its blades with a fully submerged configuration that encloses the power conversion system, well inside its enclosure. The bi-directional ducted structure helps achieve the 'Venturi Effect' increasing the energy delivered to the turbine shaft. The system has a power output capability of 1 MW. It is best suited for areas where the water current velocity is predictable, maintaining higher velocities.

1.3.4.3 Free Flow Power Technology (FFPT). This company develops a ducted and integrated generator - turbine system named Smart Turbine Generator. Their latest project is located in the Mississipi River. This project is very similar to the one explored in this article because it is a direct-drive permanent magnet generator, designed to operate for a wide range of water velocities. The blades measures 3 m in diameter whereas a 1.4 m diameter blade is still under testing. Twenty-five of their projects have been approved

in the Mississipi River so far, accounting to 3,303 MW and 43 are still pending which will amount to adding 5371 MW more [28].

Many other innovative projects with both horizontal axis and vertical axis turbines, considering their environmental effects and other factors have been reviewed in [15].

1.4. ELIMINATING THE GEAR BOX

Mechanical power from the turbine is transferred to the electrical generator through the powertrain. This power-train typically contains a low speed shaft, a gearbox, and a high speed shaft; the generator is connected to this high speed shaft. The gearbox is intended to primarily multiply the speed of the turbine up-to ten times (or more) so the generator can function at its marked ratings. Various factors influence whether or not gearbox will be used, including reliability, losses, generator type (either direct drive or not), available space, percentage of total investment (to go in the gearbox), and so forth. Gearboxes for turbines in both the kW and MW range are often bulky and costly. Additionally, they are often found to be the weakest component of the power-train. Hence, as the system rating moves below the KW range, the gearbox is eliminated and direct coupling is considered instead. Article [29] offers a detailed discussion based on these factors as relevant to commercially employed gearboxes.

Today's turbines (with gears) are designed with a single planetary gear system and two parallel shaft helical gears. The previous models included spur gears, bevel gears, crossed helical gears, hypoid gears, and worm gears. These are listed in the decreasing order of preference based on their rolling and sliding action. Several

lubricating methods are in use [30] allowing for a smoother functioning and fewer failure of parts. The Continuously Variable Transmissions (CVT) and the Magnetic Bearings are viable competitors to conventional gears. Each provides tremendous flexibility in gear ratios. Due to this fact they have achieved mass production lately. While both are promising technologies, CVTs' fail to handle higher torques and magnetic bearings on their huge magnet requirements. Additionally both are outrun by direct drive and torque splitting solutions that offer higher efficiencies and unmatched reliability.

Gear failures are not always a result of human error or gear tooth design. They are also not specific to either a particular designer or manufacturer. They constitute to only about a 10 % of total failures. The majority of failures occur because the ball bearings fail [31]. These bearings develop minor cracks that lead to micro-pitting and cracking. These issues will eventually cause the bearings to break apart. This microscopic debris not only contaminates oil and grease but also begins to misalign the bearings themselves. These bearings then become skewed, leading to a host of additional problems. The real culprit, however is the severe torsional stress [32] from the turbine. It is generated in the event of an emergency shut down or reversal or any related severity from the grid side.

Extensive solutions have been proposed [30, 33] to prevent failures. It is perhaps inevitable, however that mechanical components will fail; even the best performing devices have a fixed lifetime. Additionally the need for routine maintenance will continue to increase as the size of both the turbine blades and gear box increases. Because higher the torque generated, larger the gear box size. Hence, the gearbox should be completely removed from the system. Doing so would result in a weight reduction of the turbine head. Eliminating the purchase and maintenance expense of these high performance

gearboxes also saves a great deal of money. At present, gearless direct drive wind turbines are commercially available in a number of other countries including Europe. These turbines can operate at a low speed range of 12 to 30 rpm.

Low power generators allow for fewer losses in electro-mechanical devices i.e., either the gearbox during energy transformation or during speed increase. These losses can include losses in the speed-up gear, bearing losses, and windage losses. The power delivered as input to the generator is calculated by subtracting these mechanical losses from the turbine mechanical power output.

The expression for finding the losses in a gearbox for either PMSG or DFIG [34] is:

$$P_{gear} = P_{gearm} \frac{N_{actual}}{N} \quad (1)$$

The gear loss is normally around 3% to 5% of the generator's rated power. A loss of 0.5W is considerably high for a low power generator (i.e. 10 W). Hence this stage must be eliminated effectively. At the same time new systems must be developed by directly coupling the generator to the turbine blade structure. Doing so would reduce the number of both active and moving parts, eliminating losses and improving efficiency by up to 96% [35] in kW rated machines. Many such direct drive topologies have been presented [35-37]. The efficiency numbers can be compared with that of conventional gearbox technology results when choosing whether or not to use a gearbox.

This gearless system sometimes called the Direct Drive PMSG, yields the highest power output [37] if directly coupled, thus eliminating the gearbox arrangement. The direct coupling does, however, increase the cost, and make the system quite expensive.

The generator designed in this article is for an in-house built hydrokinetic turbine with a maximum speed of 300 rpm. A directly coupled PMSG was designed and built for this purpose. It was rated at 240 rpm, eliminating the gear box and falling under the direct drive category.

1.5. PERMANENT MAGNET TECHNOLOGY

The use of permanent magnets on the rotor eliminates both the complexity of rotor windings and rotor copper losses, resulting in a simple structure with increased efficiency. The number of magnets used is equal to the number of poles. The number of poles increases when the PMSG is operated at lower speeds. The cost of an electrical machine depends on many parameters i.e. material cost, production line processes, number of parts, and amount of copper used.

Most of the emerging renewable technology solutions for electricity generation, from linear generators to direct drive PMSGs use permanent magnets. The material cost is a major factor here because the magnets are expensive. These magnets are made from rare earth materials, such as Neodymium-Iron-Boron (NdFeB), Alnico, Bonded Neodymium, and Samarium Cobalt (SmCo). They have excellent physical and magnetic properties [38-40], inlcuding high remanence and coercivity, excellent thermal stability, high resistance to demagnetizing influences, corrosion resistance, and high energy product.

The volume-to-specific-energy $\left(V_2 S_E\right)$ ratio of the magnetic material is an important measure of magnet strength. Just a decaded ago, ferrites were the common choice. Recently NdFeB magnets have gained attention since they have ten times higher

V_2S_E ratio than do ferrites. Because NdFeB magnets have the highest energy product (from 26 MGOe to 54 MGOe), they are the outstanding choice for PMSG applications. Unfortunately obtaining these rare earth materials is expensive as they are not readily available in the US; they must be imported from other countries [41]. While it seems a simple option from a research point of view to import at cheap tariffs and make use of the material extensively, from an industrial perspective it has a lot of implications ranging from military restrictions to political and economic requirements.

A great deal of research has been conducted [42] to identify not only better magnetic materials but also better electromechanical structural solutions [43]. Samarium once cost three to four times that of Neodymium measured in cost/year for ‘n’ pounds of the material. Recent studies [44] have provided a great deal of importance to find more profitable magnetic materials with high energy density. These new materials are engineered at the nano level, forming both nano-composites and nanostructured magnets. Thesed developments have led to various interesting and new hybrid magnets with materials mostly available locally. These advancements give hope to low power and low speed small scale machines such as the one constructed in this article. There are also ultra high temperature (UHT) and superconducting magnets being researched for MW – GW range machines which offer other advantages.

The common notion is that higher voltages can be achieved by increasing the size (thickness) of the magnets. Magnet thickness however is limited to 11-12 mm [45]. The open circuit phase voltage produced remians fairly constant, for magnets thicker than this value. This factor must be considered when a PMSG is designed. It also justifies the need for research into a better magnetic material.

1.6. MOTIVATION FOR THIS THESIS WORK

Permanent Magnet Generators have been employed for many decades due to its application in both wind and hydrokinetic turbines. These generators are a low cost solution for a stable, reliable, and efficient power output. The simple design leads to a lower weight of the machine and reduced maintenance as compared to either a DC machine or a slip ring induction machine of the same power output. This allows the PMSG to run satisfactorily for years.

Most applications assume a gearbox will maintain a speed between 1800 rpm and 3000 rpm. This operating range becomes 150 rpm to 600 rpm for a direct drive system, the natural rotating speed of either a water wheel generator or a hydrokinetic turbine [46]. A very low rated speed (240 rpm) was considered for this project. This speed is a mechanical constraint of the custom built turbine. The primary concern in obtaining a generator for this speed is that very few companies build PMSG for such low speeds because the price of constructing a generator is inversely proportional to the machine's rotation speed.

A technical reasoning for the above mentioned fact can be provided as follows. From the basic equation of rotating machines,

$$N = \frac{120 \cdot f}{P} \tag{2}$$

It can be seen that, as speed decreases, for a fixed/pre-determined frequency of the synchronous field, the number of poles will increase. Thus the number of magnets on the rotor must be increased. Subsequently, a larger magnetic field is required to produce

higher power (the higher the flux, the higher the voltage induced and, hence, the higher power produced) for a given number of poles. It is governed by the equation,

$$\phi_g = B_{av}\left(\frac{\pi DL}{P}\right) \tag{3}$$

Rare earth magnets are expensive if stronger Neodymium (NdFeB) magnets are used (as in most recent applications), then the total cost to obtain magnets of required size and shape.

$$N_s = N_{spp} N_m N_{ph} \tag{4}$$

Increasing the number of poles increases the number of slots on the stator justified by equation (4). Increasing the slot number reduces the tooth ripples. Unfortunately it also contributes to both a weaker stator tooth and a more complex stator structure. Additionally increased winding resulting in an increased use of copper [46]. Manufacturing a complex stator and winding the coils is a tedious task, particularly if it must be constructed in-house (as demonstrated in this thesis report). Altogether, increasing the slot number increases the overall cost of the machine.

Novel solutions are available for low speed requirements [35, 37, 45, 47, 48]. It should be noted, however, that each design was built to serve in either the kW or MW range.

Starting torque also must be considered. As the size of the generator increases, so does the mass of the rotor. A corresponding torque needs to be applied to overcome both the inherent inertia and the load torque of the rotor mass:

$$T_e - B_m \omega_{rm} - T_L = Jp\omega_{rm} \tag{5}$$

The turbine output shaft provides the torque required for rotor rotation. Because the maximum torque the turbine can produce is 0.08 Nm, the mass of the rotor cannot exceed a particular value.

$$\Sigma\tau = I\alpha \tag{6}$$

$$I = \Sigma Mr^2 \tag{7}$$

Another problem is the unavailability of off-the-shelf magnets with the required length and inner diameter. These magnets can be almost impossible to find if the number of pole pairs increase and the skewed magnets are designed.

The size of the machine is directly proportional to the power requirement. The water wheel generator inherently has a larger diameter and a shorter axial length. Hence, these machines are known as vertical axis machines. As a result of the previously mentioned constraints, the stator structure is diametrically constrained. The unavailability of skewed magnets also limits the flexibility in reducing the cogging torque [49].

Designing a generator with minimal expense while retaining the ability to harness sufficient power and have the highest amount of efficiency possible was the objective of this study.

2. DESIGN PROCEDURE

2.1. POLE & ROTOR DESIGN

The magnet poles of the BLDC is similar to that of a salient pole synchronous alternator but houses permanent magnets instead of windings. In this article and article [50] a surface mounted magnetic rotor is designed. The permanent magnets so chosen must possess sufficient residual flux density, magnetic coercive force and deliver higher power density. The choice also depends on the lower cost, thermally, magnetically and chemically stable magnet material available in desired sizes. It is found that Neodymium magnets satisfy most of the above requirements.

The inner diameter and the arc length of the magnet, decides the outer diameter for the rotor body. However the number of poles needs to be chosen to decide upon magnets. Low speed, low power synchronous generators usually have 8 to 12 poles. Here a 12 pole rotor with N45H grade NdFeB magnets are chosen with characteristics provided in Table 2.1.

Table 2.1: Magnet properties

Residual flux density [KGs]	13.7
Coercive force [KOe]	> 11.4
Max energy product [MGOe]	42 – 45
Physical dimensions [mm]	43 o.d; 39 i.d; 5 Lm

This hypothetical outer rotor diameter can be used as a starting point for further dimensioning. The maximum rotational speed of the hydrokinetic turbine is limited to

240 rpm. This results in a synchronous field rotating with 24 Hz frequency using the basic relation in Equation 8.

$$f = \frac{P \times N}{120} \tag{8}$$

The rotor pole pitch and stator pole pitch are essentially the same and is calculated as:

$$\theta_P = \tau_P = \frac{2\pi}{N_M} \tag{9}$$

The amount of rotor surface area covered by the north and south poles of the rotor is termed as 'embrace'. Normally the embrace is valued 65% to 80% is allowed [51]. Pole embrace affects the voltage waveform, torque ripple and leakage-flux factor. Here 90% embrace value is considered since magnetic flux leakage is low and yields a higher voltage. The extended radius value due to this embrace consideration is calculated with the help of new arc length given by:

$$S_e = 1.1(S) = 1.1\left(M_{ir}\theta_P \frac{180}{\pi} \right) \tag{10}$$

$$R_e = \frac{S_e}{\left(\theta_P \frac{180}{\pi} \right)} \tag{11}$$

The outermost rotor radius, R_{ro} includes thickness of magnets added to the rotor radius and is used for further calculations. The depth of the rotor steel, from the magnets to the shaft, is equal to the back iron thickness on the stator, which is explained in detail in the stator design section.

'Cogging torque' or 'cogging' is caused due to the symmetry/interaction in the geometry of the stator and the rotor. It is given by

$$T_{cog} = -\frac{1}{2}\phi_g^2 \frac{dR}{d\theta} \tag{12}$$

There are several ways to reduce cogging torque by making either the stator or the rotor asymmetric. Adding pole shoes which is already a part of the design, introduces asymmetry but cogging still remains significant. Lengthening the air gap is the next simplest and conventional approach. Normally rotational generators allow around 2mm air gap. In this thesis a larger 4 mm air gap is chosen both to ease manual hardware assembly and to reduce variation in air gap reluctance. Other structural solutions like skewing the rotor magnets, skewing the stator poles and having a fractional pitch winding, all of which attempt to reduce the rate of change of air gap reluctance with respect to the pole pitch, are not explored here, mainly because of the difficulty in fabricating the hardware locally and winding the stator.

2.2. STATOR CORE DESIGN

The stator of a BLDC can be divided into three main sections namely slot, stator tooth and the back iron. There is a magnetic flux linkage from the magnets to the stator and this flux needs a path to flow from one pole to the other. The back iron provides this path and hence it needs to be wide enough to sustain magnetic saturation. Normally steel saturates at around 1.5T and the flux density is limited to 1.1T to 1.3T in reality. The back iron width is calculated using

$$\omega_{bi} = \frac{\phi_g}{2B_{max}k_{st}L} \tag{13}$$

Since the number of poles is fixed and number of phases is 3, the only parameter which decides the number of slots is N_{spp} . Each slot houses a winding of one of the three phases and links to magnet poles. If flux from each magnet pole has to interact with one slot from each phase, it implies $N_{spp} = 1$, and is chosen in this design.

Using equation (14) yields a 36 slot stator for the BLDC. N_{spp} can be changed to other integral numbers but depends on the slot and stator geometry desired and its after effects. Article [51] demonstrates the effect of choosing N_{spp} for better performance but cannot be incorporated in this paper due to mechanical constraints. Increasing number of slots reduces leakage reactance and decreases tooth ripples. But there are many disadvantages to having too many slots. It increases the cost of production, makes the tooth weaker and leads to higher flux density accumulation in the tooth. Also considering the limitation in slot pitch length, 36 slots are decided suitable for the considered low voltage machine.

Once the number of slots is found, the slot shape and dimensions have to be designed. The slot pitch is used to find the major slot dimensions and is given by:

$$t_s = \frac{\pi D}{N_s} \tag{15}$$

where, ‘D’ is the inner diameter of the stator body. The slot pitch helps in winding the 3 phase winding onto the stator.

2.3. SLOT DESIGN

There are four aspects to slot design. They are the tooth width and slot height, slot opening, the slot shoe or lip dimensions and the slot shape. The conventional slot shape is the 'U' shaped wide base employed in most of the standard generators/motors. Here a different shape is developed which is more towards being conical, an advantageous shape as described in [52]. This new design holds the windings close to the rotor magnets and also contributes to better space utilization in the slot. Because the conical shape is not viable for hardware fabrication, the shape is instead an inverted trapezoid.

The tooth width is calculated based on the fraction of the back iron required to accommodate the flux contributed by each pole. It is given by:

$$\omega_{tb} = \frac{2\omega_{bi}}{N_{sm}} \tag{16}$$

$$N_{sm} = \frac{N_s}{N_m} \tag{17}$$

Initially the slot width at the base is taken equal to the tooth width to start with design and later optimized based on winding requirements and tooth back iron requirements as the slot takes shape. This optimization is done in RMXprt® as described in further sections. The slot depth fraction, α_{sd} varying between 0.4 - 0.5 is used to calculate the lip dimensions. The idea of providing a lip to the tooth is to increase the surface area for the flow of flux in the stator tooth, as much as possible. In conventional generator slot shapes, this lip takes a two-step design approach in the cylindrical type slot shape. The inverted trapezoid idea limits this approach since it invades the winding space inside the slot. Hence a single step is provided.

The optimized height of the slot is decided based on the number of turns of winding required and the corresponding area occupied/demanded. Based on the slot depth/height finalized, adding the width of back iron to it gives the total outer diameter of the stator. This diameter and dimensions can be scaled up as and when higher power is required using the discussion above.

3. MACHINE SIMULATION

Once the machine is designed and before hardware is constructed to design specifications, it needs to undergo both performance optimization and heat and magnetic saturation test. This is carried out through the ANSYS software – RMXprt® and Maxwell 2D®. Thus the process of machine design is always iterative. The advantages of using and the mentioned software and the method of implementation are discussed in the following sections.

3.1. SIMULATION IN RMXprt®

Rotational Machine Expert or RMXprt® is an interactive software package used for designing and analyzing electrical machines. It is a convenient way to speed up the design and optimization process of rotating electric machines. It has a plug and play interface and makes it easy to build the machine quickly. Its graphical user interface (GUI) is user friendly since it allows changes to entered machine parameters and viewing corresponding changes immediately. This provides for multiple simulations and is very helpful in making sizing decision and also during optimization in a short span of time.

The RMXprt library contains many types of rotating electric machines stored as plug and play interfaces. It not only contains the machine definitions but also includes the power electronic and control circuitry that might be associated with it. There is provision to add any other complex circuitry desired by linking it to Simplorer® and hence editing the circuit. Once the performance curves are verified for satisfactory performance, the same design can be exported to Maxwell 2D or Maxwell 3D to analyze the mechanical

and electromagnetic characteristics of the machine using Finite Element Analysis (FEA). Both magnetostatic and transient analysis can be conducted. Since RMXprt simplifies the simulation environment to such a great extent, it is chosen to simulate the Brushless DC machine being constructed in this project.

The procedure followed to create an RMXprt drawing and simulation of the machine is discussed here onwards. Since RMXprt is built upon the core of Maxwell 2D, the RMXprt design template needs to be inserted first in Maxwell. Once the template is inserted, the type of machine needs to be selected. Since it is attempted here to get a DC type trapezoidal output, a Brushless Permanent Magnet DC motor is inserted. Various stator, rotor and control circuit tabs are inserted into the file as can be observed in Figure 3.1. Each of these tabs display machine design parameters to be keyed in. These values are obtained as described earlier in the design process.

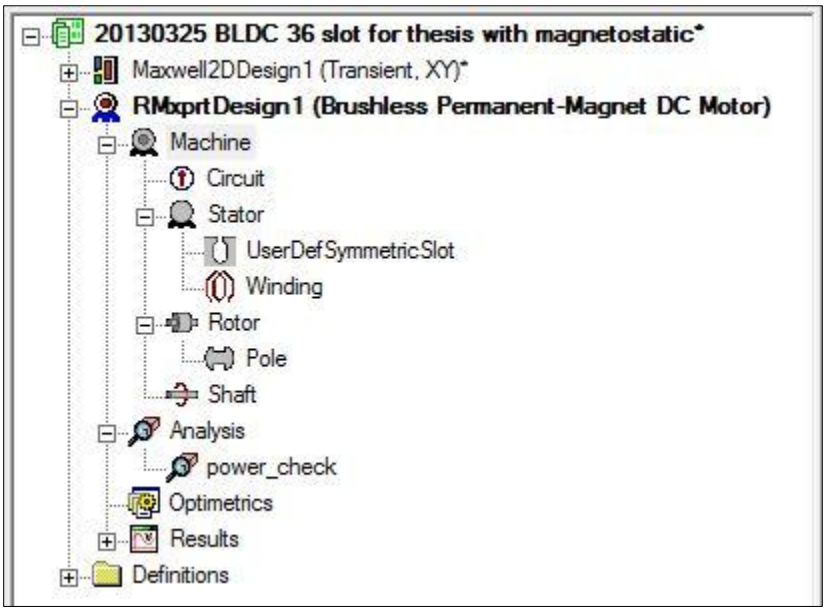

Figure 3.1: Snapshot of the RMXprt interface

The goal was to design a 12 pole, Brushless DC generator that has a reference speed of 240 rpm, which is the rotational shaft speed of the water turbine. A ‘Y’ (Star) connected circuit with a three phase full wave full bridge rectifier is desired to convert synchronous AC into DC. Hence a DC control circuit option is selected. All of the above data is entered in the ‘machine’ tab. In the circuit tab, the control approach for the bridge is specified with a 0^{o} lead angle and 120^{o} pulse trigger.

In the stator tab, the mechanical dimensions and the number of slots are specified. The material type for is chosen to be M19_24G. M19_24G stands for M19 type of steel with 24 gauge thickness. The M19 steel is a type of high grade silicon steel also known as Electrical Steel. It is also the most commonly used grade of steel for motion control products. It has the beneficial properties of low core losses and minimal eddy current circulation [53]. More description of the steel properties and its usage is provided in the hardware construction section.

Another important thing in this tab is to choose the slot type. Since in this document a new type of slot is designed, the ‘user defined slot’ option is selected. This allows defining the dimensions, the tilt angles, the shape and all other parameters of the slot to be defined individually. The slot geometry and the design values are provided in Table 3.1.

By now RMXprt would have generated the stator structure based on the specifications. It is essential to connect all coils manually which displays how the coils can be wound and also the slot combination based on the slot pitch. The winding diagram (also called winding layout) can be visualized in Figure 3.2.

Table 3.1: Slot geometry & nomenclature

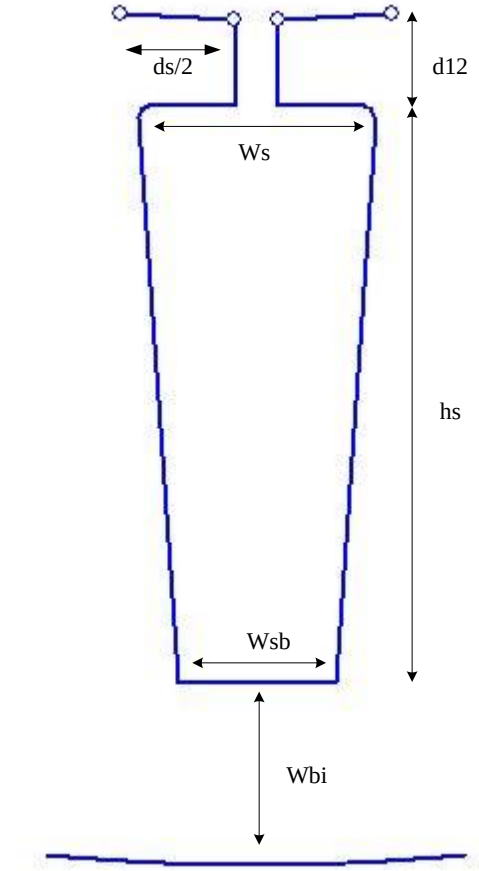	d_s	Lip width	0.8 mm
	d_{12}	Lip height	1.52 mm
	h_s	Slot height	10 mm
	W_{sb}	Slot bottom	2.6 mm
	W_s	Slot top	3.8 mm
	W_{bi}	Back iron	4 mm

In the rotor tab, the corresponding rotor dimensions are entered. The material for rotor is the same M19_24G electrical steel. Poles of the rotor imply the magnets on the rotor. There are several types of pole shapes based on the type of application and the generator in consideration.

A simple adjacent type or radial pole would serve well for the BLDC constructed here as opposed to various salient type poles. The magnets are specified to be NdFe35 ($\mu_r = 1.0997;\ \sigma = 625000\,\mathrm{Sm}^{-1};\ H_c = -890000\,\mathrm{Am}^{-1}$) grade and the thickness of the

selected magnet is entered. The stator and the rotor structure so designed can be visualized as seen in Figure 3.3.

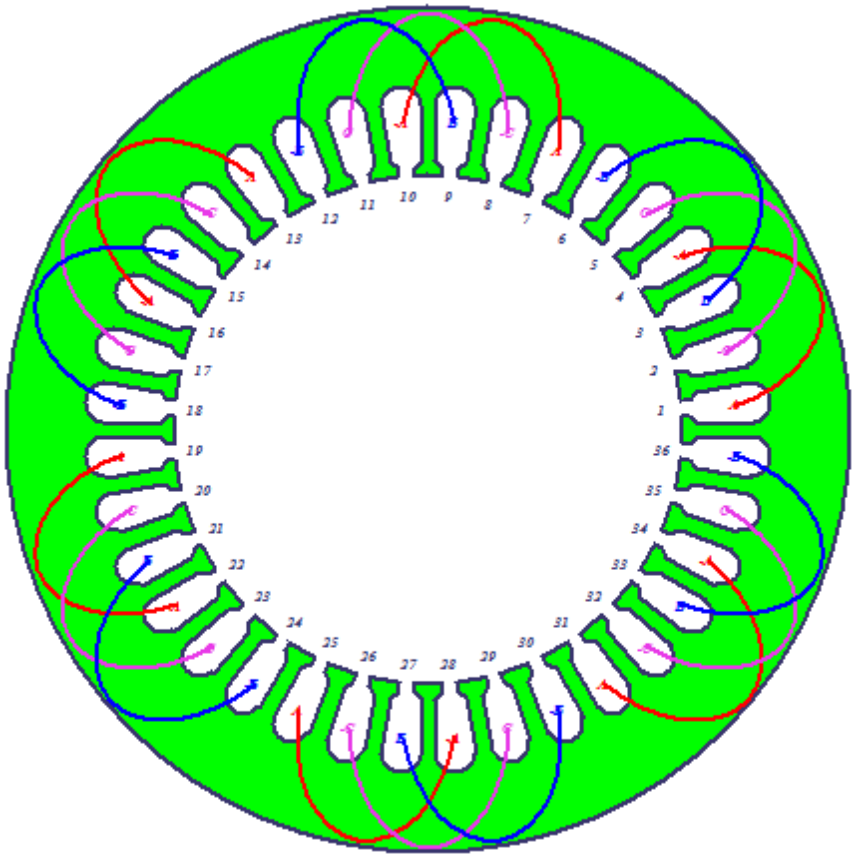

Figure 3.2: 3-phase, whole coiled stator representation

The initial analysis is conducted for specifications provided in Table 3.2 below.

Table 3.2: Machine power rating specifications

Rated Output	10 W
Rated Voltage	24 V
Rated Speed	240 rpm
Operating Temperature	75° C
Load type	Constant Speed

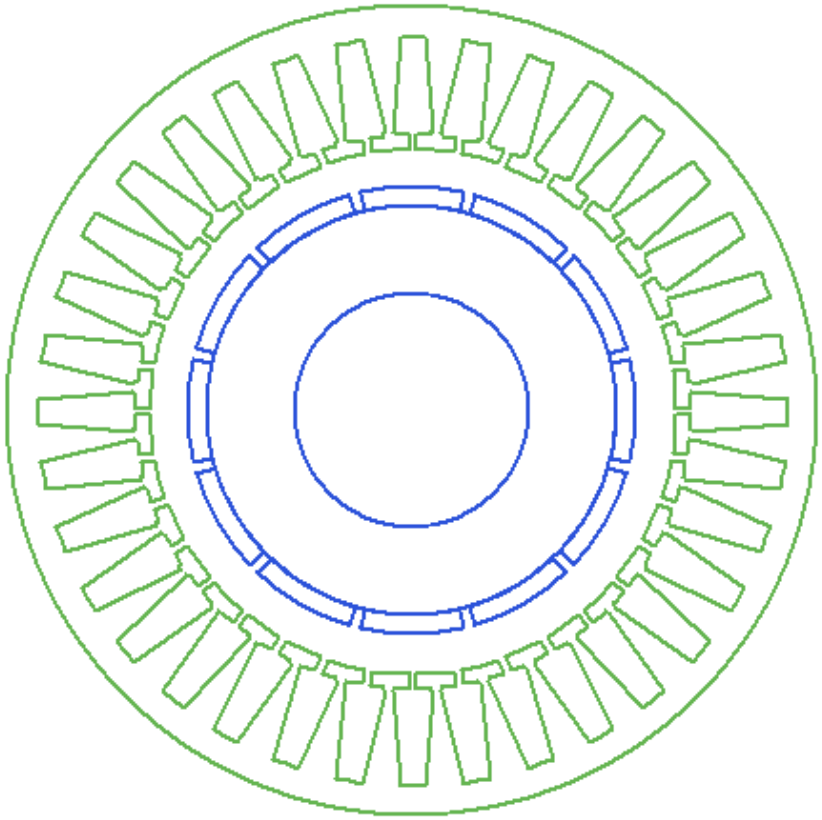

Figure 3.3: Rendering of the stator and rotor through RMXprt based on the design

The following curves are obtained by simulating the designed BLDC.

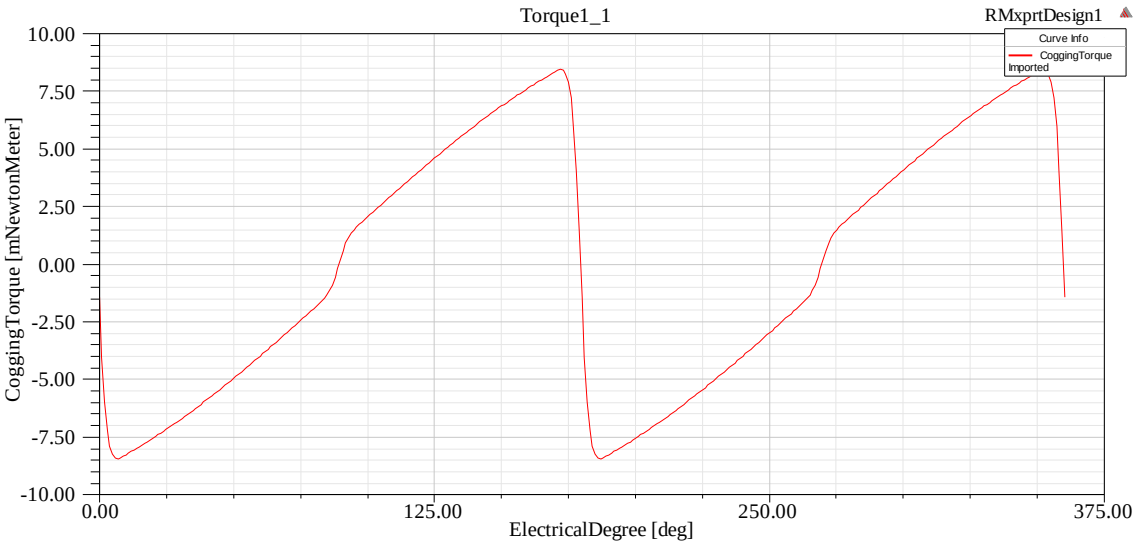

Figure 3.4: Cogging torque curve

Continuing the discussion in Section 2.1 of this document, the cogging torque causes a major problem if left unchecked. To have a comparison in values, the torque produced by the turbine is given by

$$\vec{\tau} = \vec{F} \times r = 0.12 \text{ Nm} \tag{18}$$

The cogging torque needs to be much lesser than this value for the generator to rotate smoothly and without stalling. Figure 3.1.4 plots cogging torque on 'y' axis varying along with the electrical degree of rotation on 'x' axis. It is observed from Figure 3.4 that the maximum cogging torque occurring in this generator is around 0.008 Nm.

Figures 3.5 and 3.6 are plotted for the following specifications that are aimed to accommodate the actual power output and torque specifications from the turbine:

Operation type: Motor	Rated output: 5 mW
Rated voltage: 4V	Rated speed: 240 rpm

The machine is being simulated in "Motor mode" here and the results so obtained do not necessarily represent the performance of the generator. Unfortunately RMXprt does not have an option to simulate the Brushless DC machine in generator mode. For this sole reason, the model is exported to Maxwell 2D and simulated with the correct internal circuit representation further explained in Section 3.2.

Figure 3.6 represents the efficiency curve when the machine is projected as a Brushless DC machine. It indicates a maximum efficiency of 50 % at the rated speed. It is the because of this very low efficiency that not many companies manufacture generators for such lower speeds. Also this loss calculation does not consider the losses in the electronic drive attached to make the PMSG a BLDC.

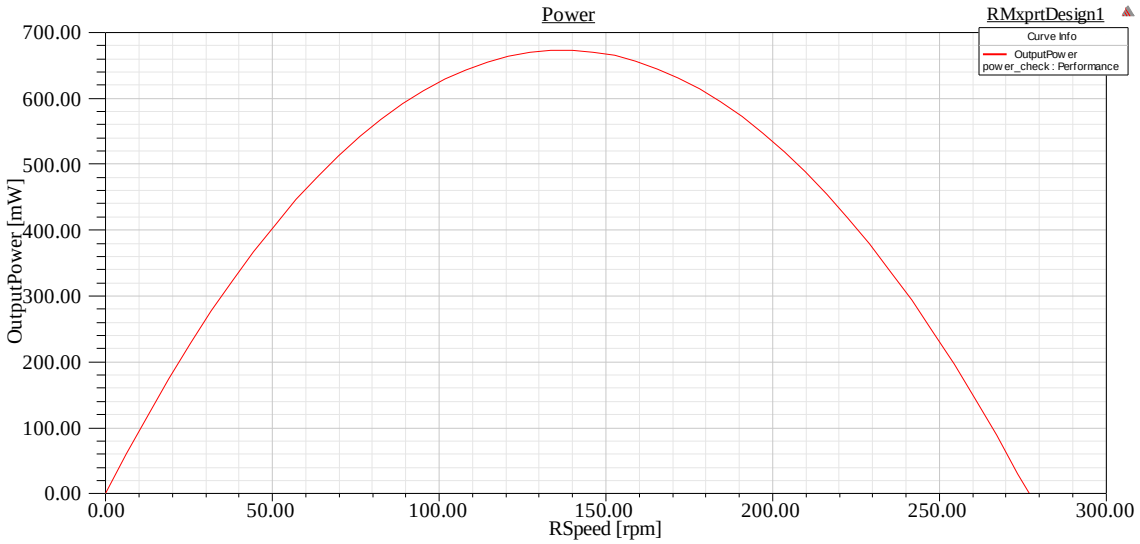

Figure 3.5: Projected power curve of the BLDC machine

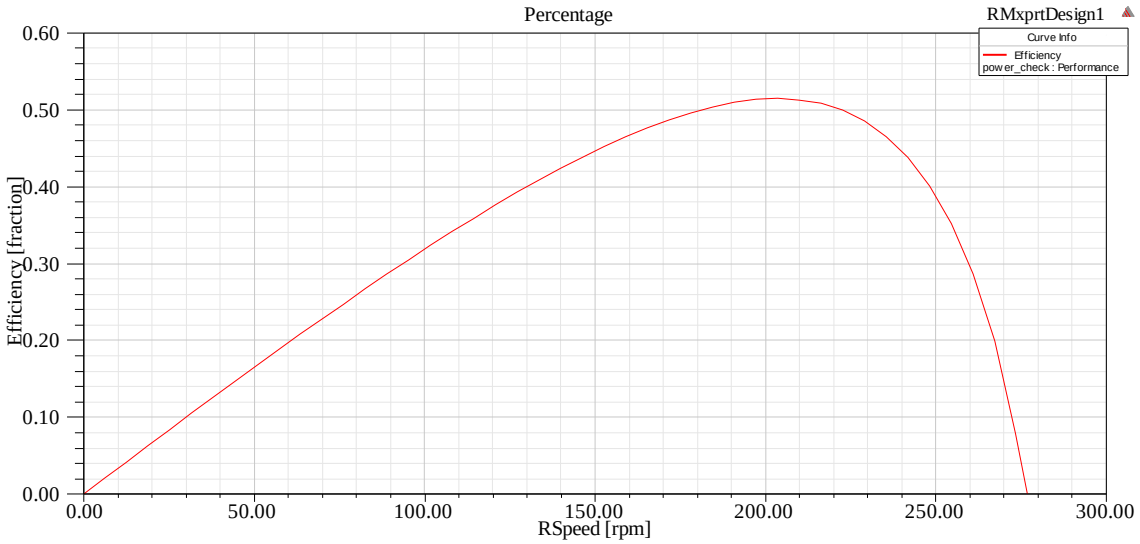

Figure 3.6: Projected efficiency curve for the BLDC machine

3.2. SIMULATION IN MAXWELL - 2D®

Maxwell 2D® uses Finite Element Analysis (FEA) techniques based on maxwell equations to solve two dimensional electromagnetic problems. Since the geometry is already fed through RMXprt® and the material already selected, the excitation is altered. The 3-phase diode rectifier circuit feeding a machine equivalent representaion is removed and a 3-phase star connected load is attached to the machine equivalent to turn it into a generator from a motor. It can be visualized in Figure 3.7.

However without the rectifier circuit attached, the machine becomes a PMSG and shall be regarded the same here onwards. As a result sinusoidal plots are seen instead of the trapezoidal waves that would appear in a BLDC. Figures 3.8, 3.9 and 3.10 show the characteristics o fthe PMSG for a 1 ohm 3 phase load.

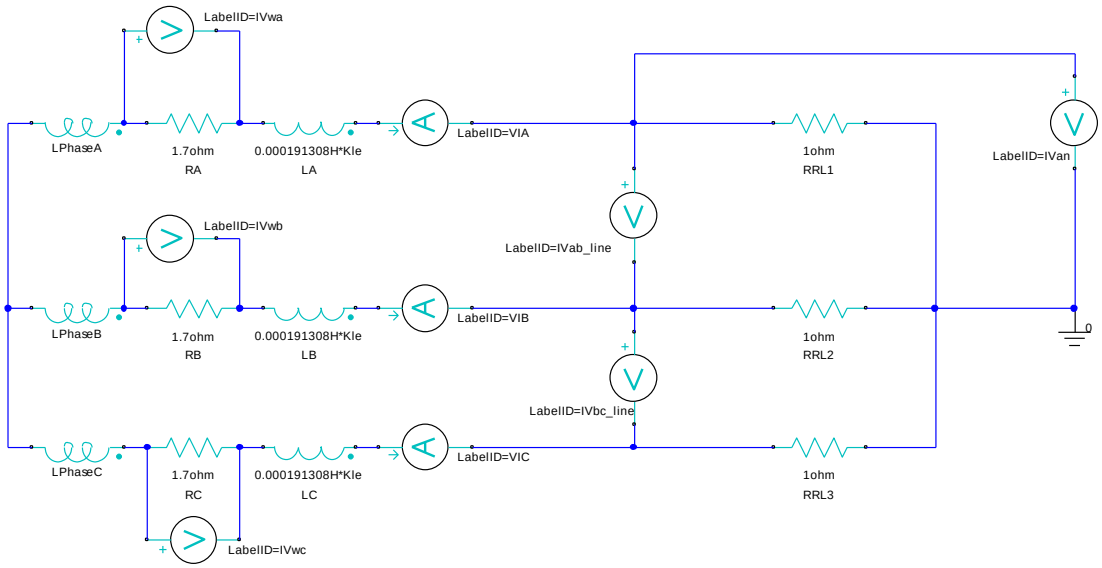

Figure 3.7: Generator equivalent representation connected to a 3-phase load

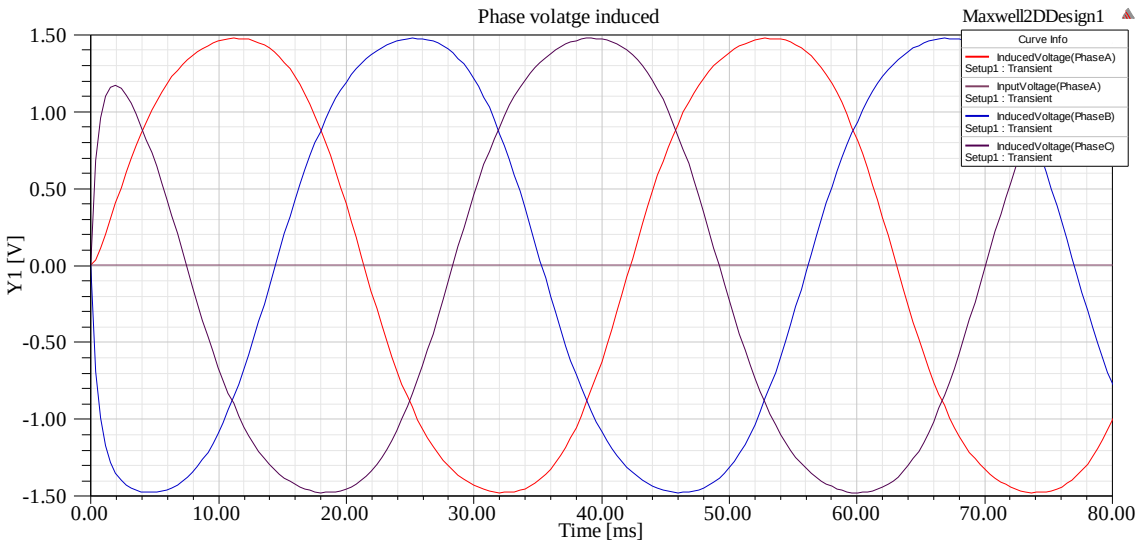

Figure 3.8: Voltage induced in each phase/ of the star connected generator winding

Figures 3.9 and 3.10 represent the supply current of the generator and the back emf produced by the generator. It is represented by meters across the equivalent winding representation as seen in Figure 3.7.

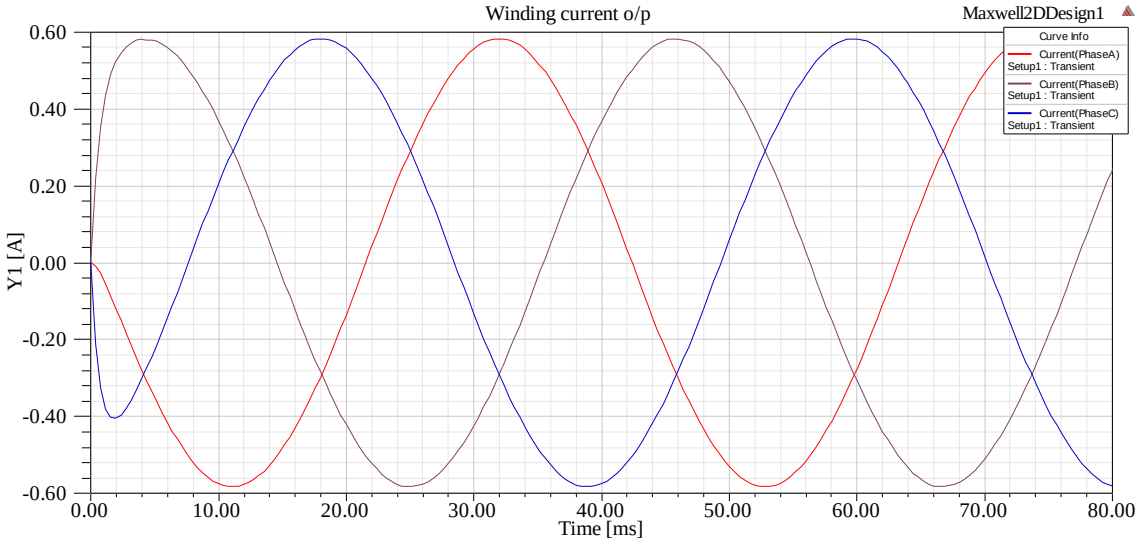

Figure 3.9: Current flow in each phase of the star connected winding

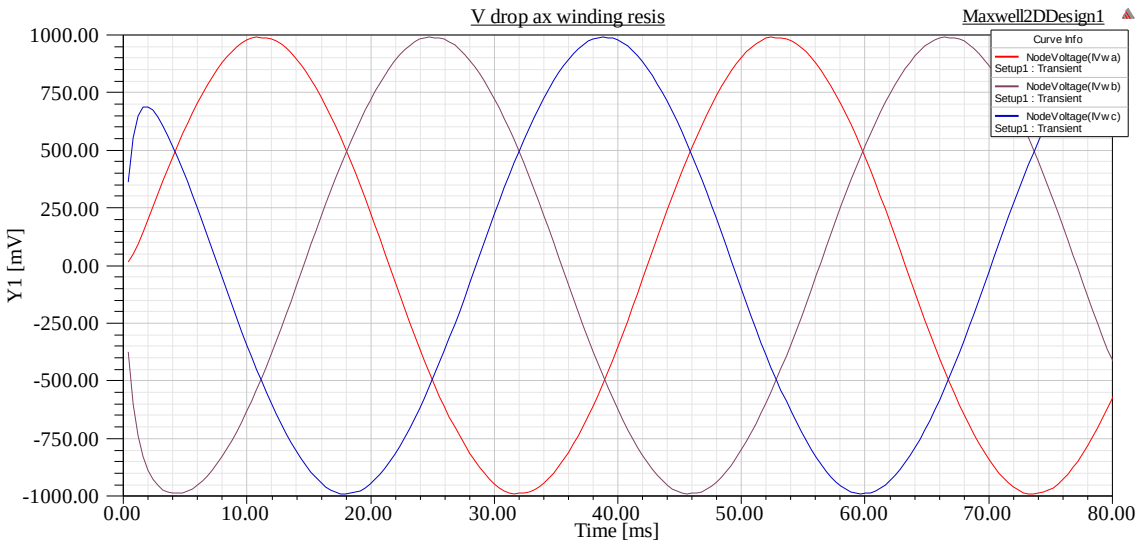

Figure 3.10: Voltage drop across the load resistance of each phase

The first thing to be noted is that the voltage waveforms are clearly displaced by 120^0 and there are no distortions due to cogging torque issue. This validates the design worthiness. Figure 3.11 represents the line to line voltages V_{ab} and V_{bc} and Figure 3.12 represents the line to neutral voltage V_{an} .

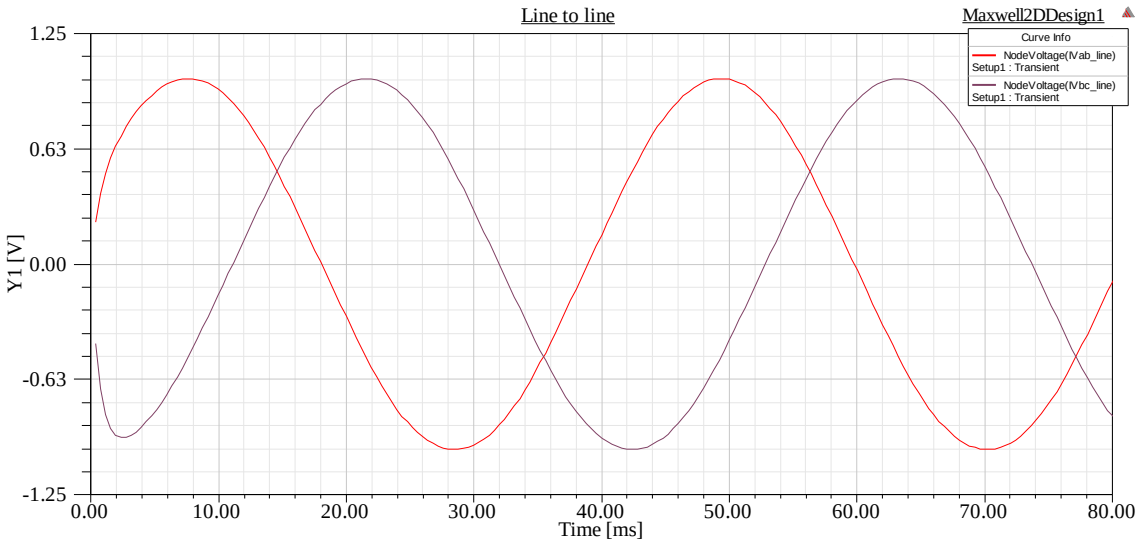

Figure 3.11: Line – to – line voltage measured between two sets of phases

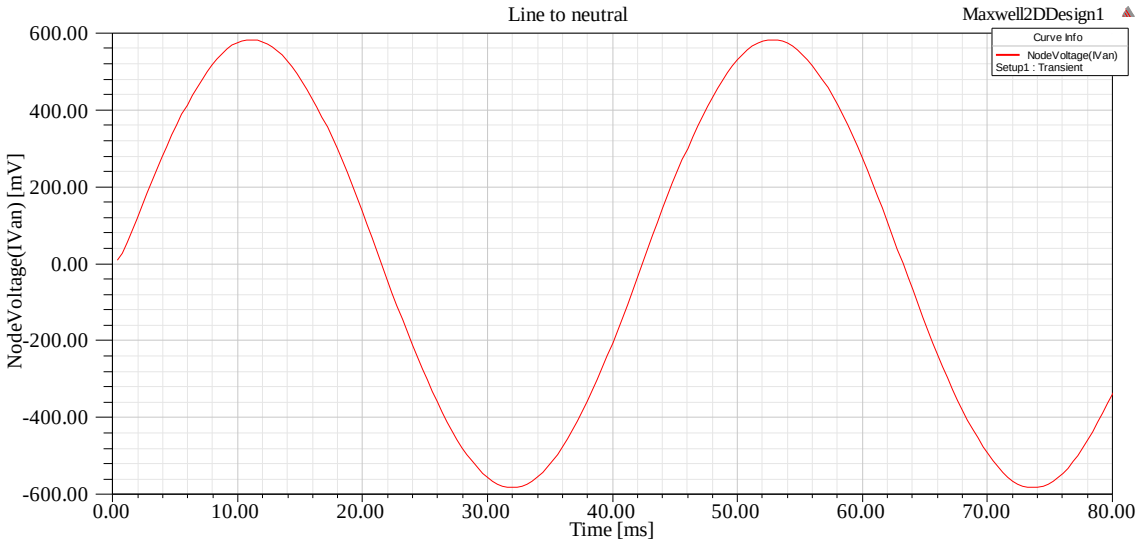

Figure 3.12: Line – to – neutral voltage (between phase A and neutral)

While the voltage and current waveforms are observed and the machine is proved to work from an electrical aspect, the magnetic aspect needs to be proved. For this reason, the model exported to Maxwell 2D® is used. Maxwell 2D® has many solvers including 'electrostatic', 'magnetostatic' and 'transient' to name a few. Electrostatic solver is used to understand static electric fields and magnetostatic solvers are used to observe static magnetic fields in the machine. But the transient solver allows us to observe and analyze the magnetic fields, energy, flux and many other parameters of a machine model at various time steps.

In this article we are interested to see the behavior of the PMSG in real time under rotational motion. As discussed previously in Section 2.2, if the back iron is designed well, it provides sufficient path for the flux generated from the magnets to get linked to the tooth and flow through the back iron around the slot. Else the flux shall be concentrated in the slot tooth and cause it to saturate/melt. It is observed in Figure 3.13.

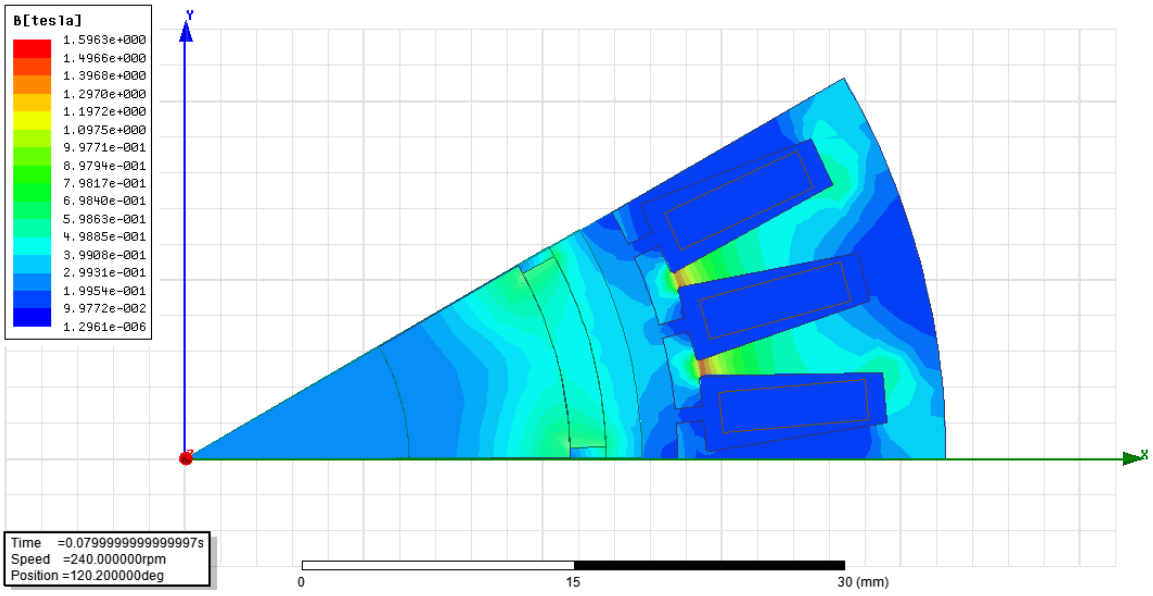

Figure 3.13: Magnetic flux density plot for one pole pitch of the generator

Considering the complexity of structure and detail for a lengthy transient simulation, it is run only for 80 ms with 0.4 ms time step. Also taking advantage of the symetricity of the rotational machine, the analysis and results for one fraction or one pole putch of the machine is applicable to the whole machine. Figure 3.2.7 shows one such pole pitch for which the flux density is plotted. It is observed that the tooth region contains a flux of almost 1.3 T. This can be harmful to the stator core. But this is only a snapshot of one time step. It can be seen in the transient animation that the flux is evenly distributed and that the stator core is not staurated.

Figure 3.14 shows the electric field line distribution for one pole pitch of the machine. It is noted that the value is slightly higher at 1.2e-3 Wb/m but is acceptable.

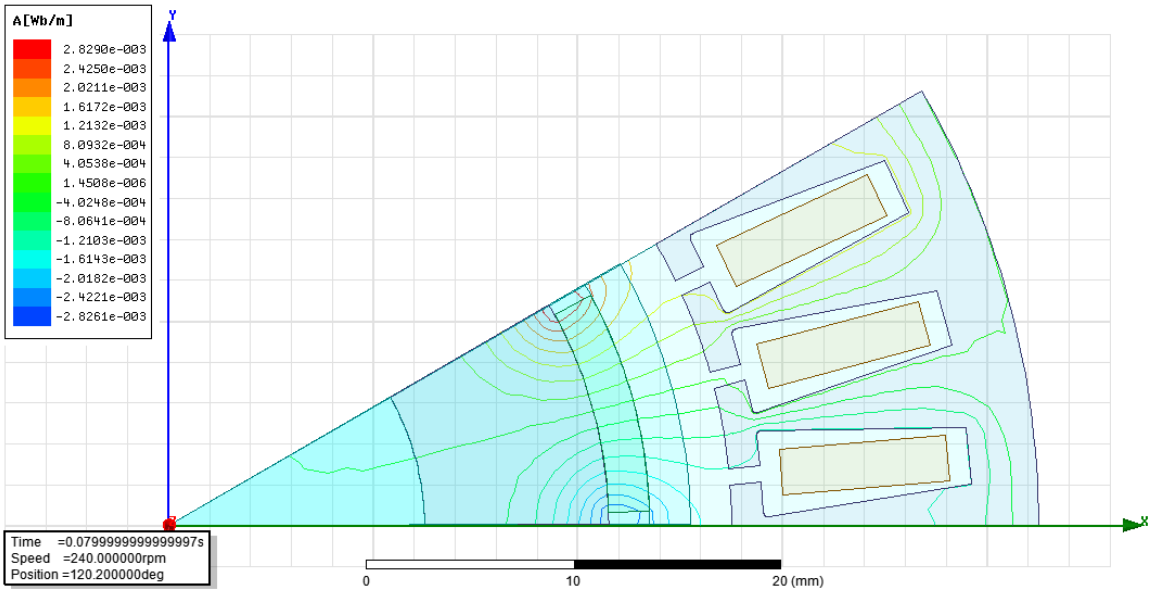

Figure 3.14: Electric Field line plot for one pole pitch of PMSG

4. HARDWARE CONSTRUCTION

The structural feature of PMSG machines is a larger face diameter and a stout length. As a result the stator measures 25 mm and the rotor measures 20 mm in length. The length of a PMSG depends on the power output required since increasing the number of magnets on the rotor leads to higher flux density linkage and hence higher voltage is induced. Since in the present design, the magnet addition does not lead to a significant increase in power as seen in RMXprt® simulation, the length is limited to above values.

4.1. LAMINATION STACKING

The M19_24G steel selected for making laminations measures 0.025 inch in thickness. The following equation can be used to calculate the number of stator and rotor laminations

$$n_{st\_lam} = \frac{L}{t_{lam} k_f} = 42 \tag{19}$$

$$n_{rt\_lam} = \frac{L_{rot}}{t_{lam} k_f} = 34 \tag{20}$$

k_f is the stacking factor with value 0.95. It signifies that only 95% of the measured stator length is actually steel whereas the rest is air in the inter-lamination distance. This is done to reduce eddy current flow and hence reduce the iron/core losses in the generator [54]. Later the compressed laminations are bolted together and heat welded to stay in place. The rotor laminations are treated in the same manner but housed on a stainless steel rotor shaft with an outer diameter (inner diameter of rotor stack) of 25 mm. The magnets are placed on the outer diameter of the rotor stack.

4.2. AUTOCAD AND SOLID EDGE RENDERINGS

The lamination designs are realized in the software Solid Edge®. Figure 4.1 visualizes all the dimensions of the stator and the rotor laminations.

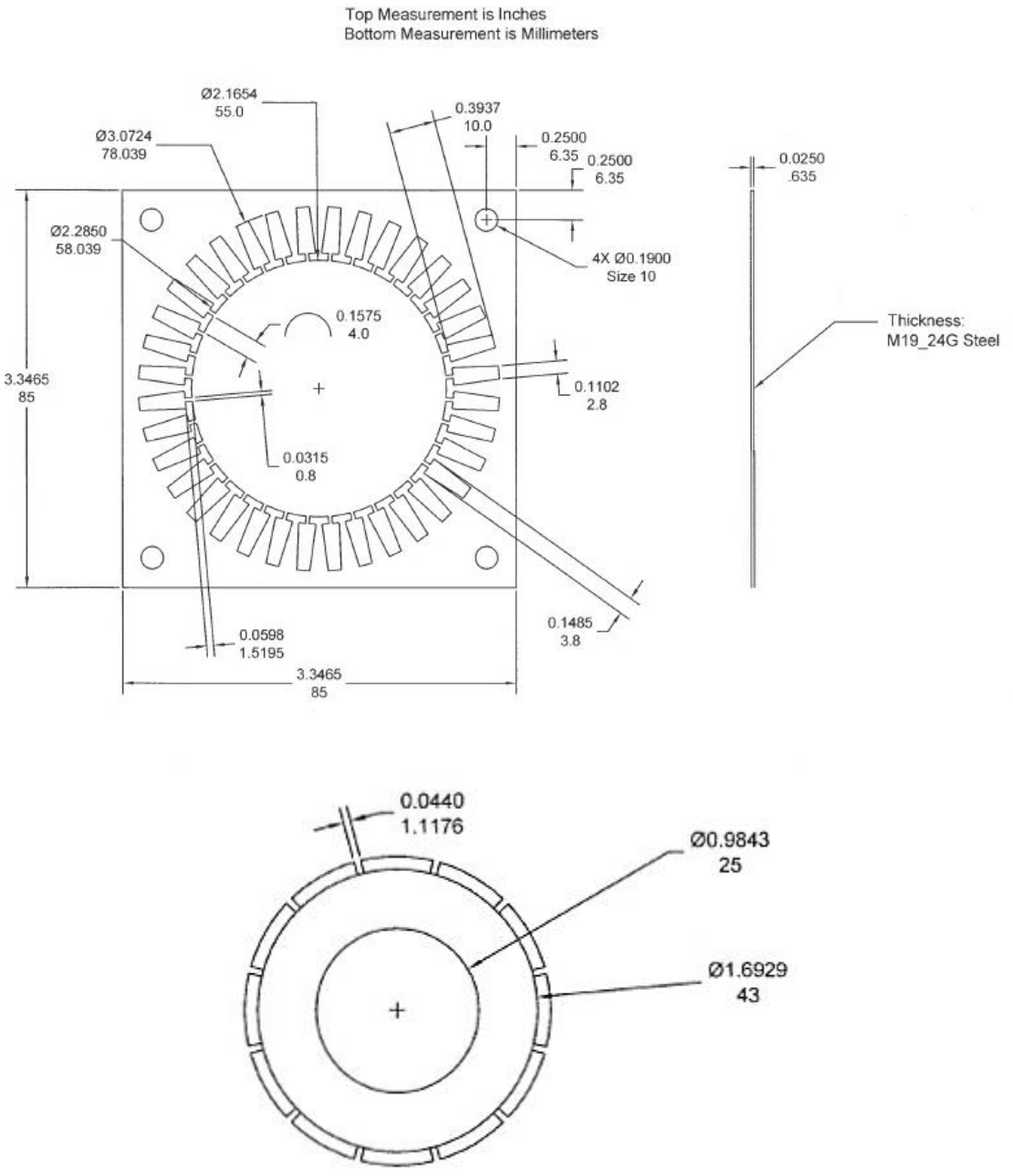

Figure 4.1: Stator & Rotor lamination design

The design is then visualized in AutoCAD® to give a 3D rendering and to aid the assembly of the generator. They are presented in Figures 4.2 and 4.3.

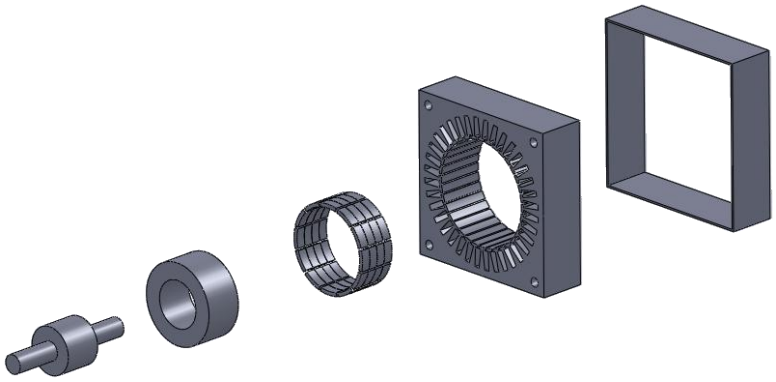

Figure 4.2: Exploded view of the generator parts

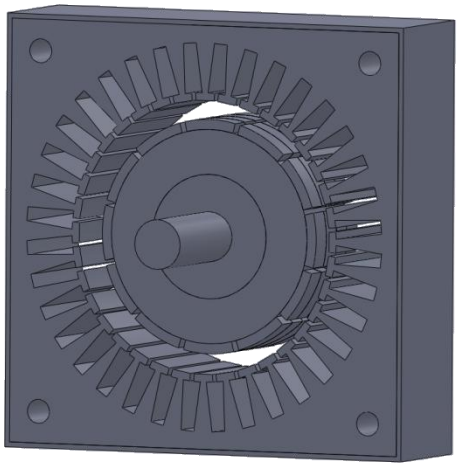

Figure 4.3: 3D rendering of the assembled generator

4.3. WINDING AND SLOT INSULATION

There is wide range of classification on how the windings can be wound [50, 55, 56] :

1. Half coiled or whole coiled
2. Wave wound or lap wound or concentric wound
3. Single layer or double layer
4. Single phase or poly-phase
5. Full pitch or fractional pitch
6. Series or parallel connection of coils
7. Integral slot or fractional slot
8. Concentrated windings or distributed windings

The back emf and force distributions are a function of how a winding is wound and pertains to specifically the region inside the slot (BLi law). Hence by changing the means of winding, the emf characteristics are altered. The machine designed in this article has a whole coiled, lap winding in a single layer, three phase winding. The windings have a full pitch arrangement and are connected in series. Since the winding is full pitch, integral slot arrangement with a concentrated winding holds good. Although parallel connection of coils is an option it is uncommon because of its possible mismatch in producing emf in two adjacent coils [50].

The fill factor is taken to be $k_f = 0.6$. The number of turns in each slot was targeted to be $n_s = 50$ according to the formula:

$$n_s = \frac{e_{max}}{N_m k_d k_p k_s B_g L R_{ro} N_{spp} \omega_m} \tag{21}$$

But due to mechanical constraints during winding, only 30 turns could be accommodated while using a 25 AWG wire. The slots are insulated with a 2 mil thick Kapton film. Varnish is applied throughout to prevent the windings from touching the stator body.

Figure 4.4 can be related to Figure 3.2 to compare the whole coiled winding. Separate connections are brought out for neutral and the phases.

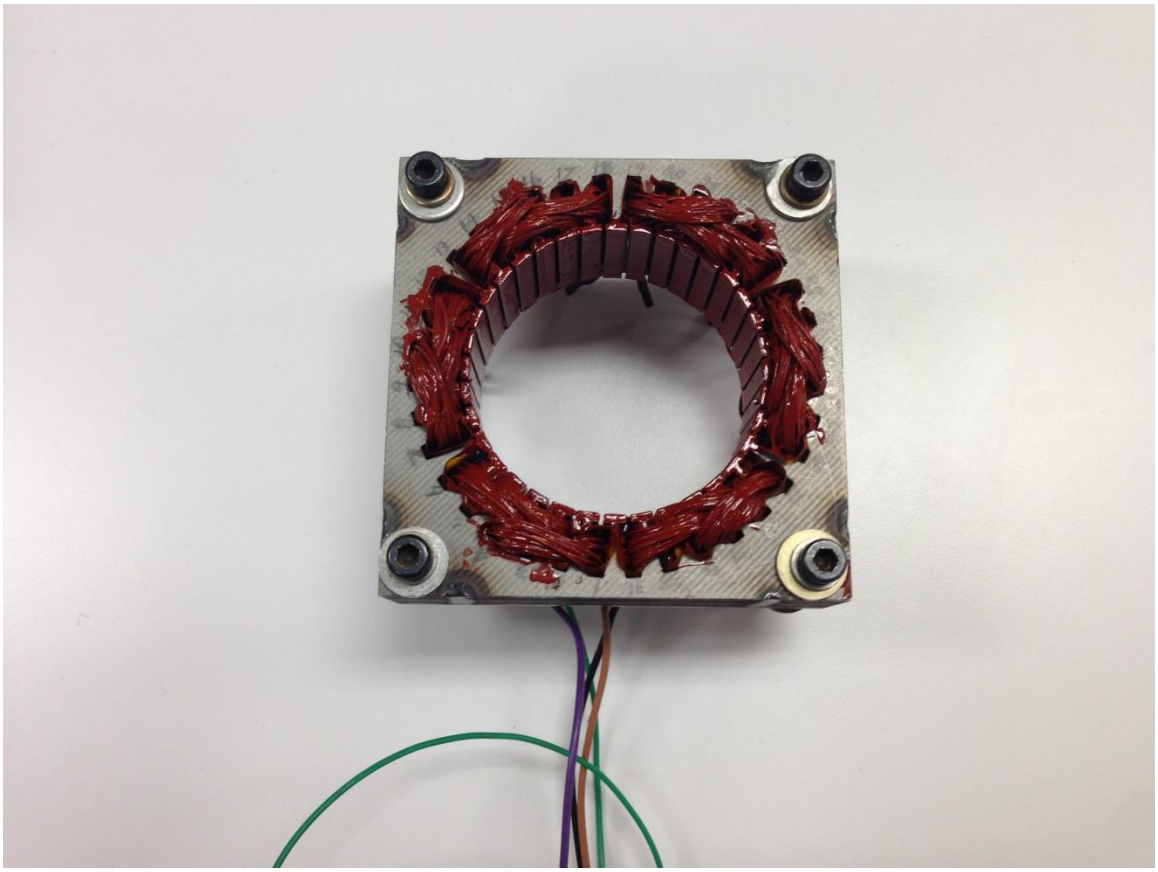

Figure 4.4: Completed stator with insulated windings

5. HARDWARE TESTING AND RESULTS

The primary concerns after hardware building is how satisfactorily or accurately it works and if it matches the results obtained in simulation. At this stage the PMSG hardware is functional but not completely built so as to attach it to the turbine. The stator and the rotor core are assembled together as shown in Section 4.2 and a temporary rotation handle is provided to carry out preliminary tests to ensure working. The hardware can be visualized as in Figure 5.1 & 5.2.

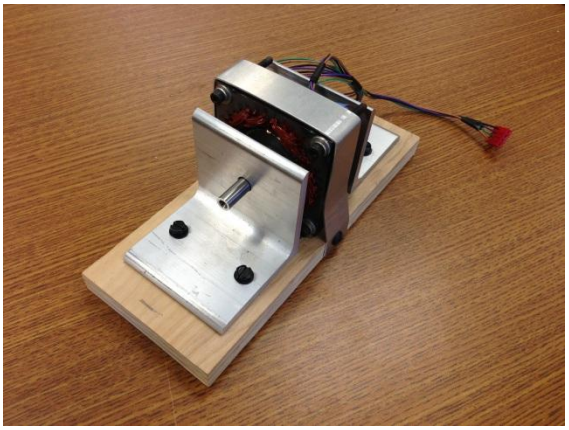

Figure 5.1: PMSG ready for testing

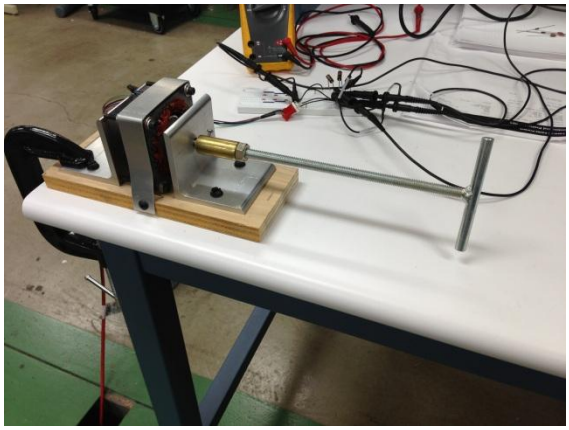

Figure 5.2: PMSG with temporary handle for rotation with a 3 phase load

5.1. THREE PHASE SINUSOIDAL WAVES

First the generator is rotated by the temporary handle as visualized in figure 5.0.2 at a speed of 4 rotations per second as obtained by the equation

$$\text{rps} = \frac{\text{rated rpm}}{60} = 4 \tag{22}$$

Figures 5.3 through 5.6 ensure that the generator is producing proper three phase sinusoidal waves phase shifted by 120^0 to each other and confirms the waveforms in Section 3.2.

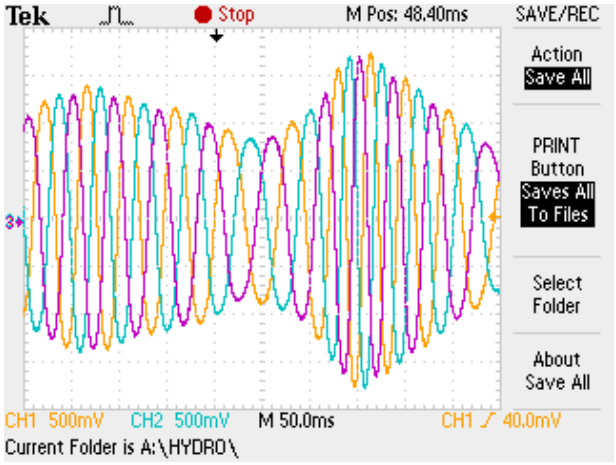

Figure 5.3: Varying frequency and varying amplitude due to varying speed of rotation

No Load condition / Open Circuit

Channel 1: Line to Neutral voltage Van

Channel 2: Line to Neutral voltage Vbn

Channel 3: Line to Neutral voltage Vcn

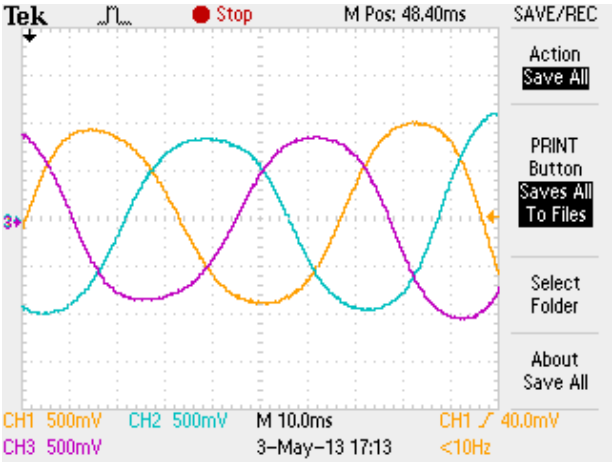

Figure 5.4: Zoomed in region of Figure 5.3. Demonstrates sinusoidal waves phase shifted by 120^0.

No Load condition / Open Circuit

Channel 1: Line to Neutral voltage Van

Channel 2: Line to Neutral voltage Vbn

Channel 3: Line to Neutral voltage Vcn

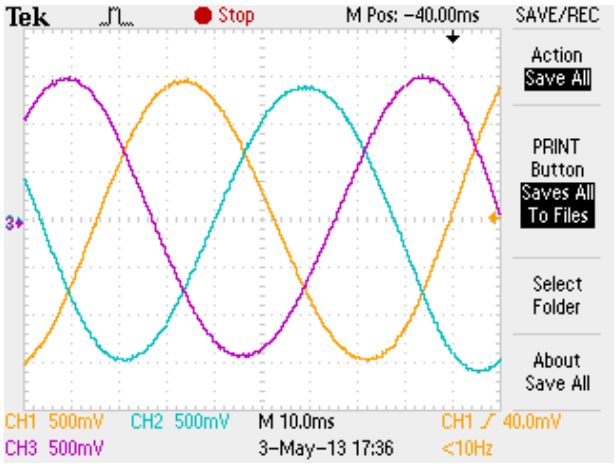

Figure 5.5: Expected 1.5V output at rated speed 240 rpm (4 rps)

No Load condition / Open Circuit

Channel 1: Line to Line voltage Vab

Channel 2: Line to Line voltage Vbc

Channel 3: Line to Line voltage Vca

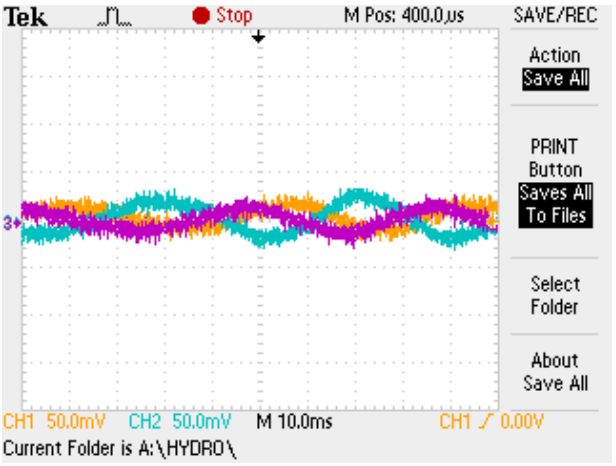

Figure 5.6: Under 1.1 ohm load in each phase of a star connected 3-phase load

With 1.1 ohm 3 phase load

Channel 1: Line to Line voltage Vab

Channel 2: Line to Line voltage Vbc

Channel 3: Line to Line voltage Vca

5.2. GENERATOR WORKING UNDER LOAD

Results obtained from hand rotation is fine for confirming that generator works but not sufficient for plotting the performance curves. Hence it is coupled with a DC motor [57] that can run upto 1750 rpm. The fact that it is a high speed motor makes it difficult to bring it down to lower speeds like 240 rpm because the motor stalls at such low speeds. Hence all following analysis is conducted at a speed of 550 rpm. The other demerit of using this machine (readily accessible) is there is no precise control over the speed. The drive used to operate this machine has an option to control the percentage of applied voltage across the armature. The speed is adjusted by controlling the applied voltage across armature and the knob controlling the current flowing through the shunt winding. The test setup is explained in the following lines.

DC motor coupled with PMSG, rotating at ≈ 550 rpm. For testing purpose a single variac load is attached to phase A of the PMSG. The load is varied from 0.4 ohm to 32 ohm and a load test is conducted. The current and voltage across the load is recorded for each variation in load in steps of 0.4 ohm until 8 ohms and then in steps of 2 ohms until 32 ohms where the power characteristics show a monotonically falling value.

The sinusoidal varying values are then converted to an rms value using the following equations where ‘n’ is the number of samples recorded (2500 samples here).

$$V_{rms} = \sqrt{\frac{1}{n}\left(v_1^2 + v_2^2 + \ldots + v_n^2\right)} \tag{23}$$

$$I_{rms} = \sqrt{\frac{1}{n}\left(i_1^2 + i_2^2 + \ldots + i_n^2\right)} \tag{24}$$

The plot in Figure 5.7 is obtained by using a value of 1 ohm in the variac. It represents the normal load condition. Figure 5.8 is under a 32 ohm in the variac and represents maximum load condition. It can be observed that the load current is maximum for low load and least for higher loads. Figure 5.7 is essentially measuring line to neutral voltage that is across the load resistance and can be compared with Figure 3.10 which is the simulation result for the same load.

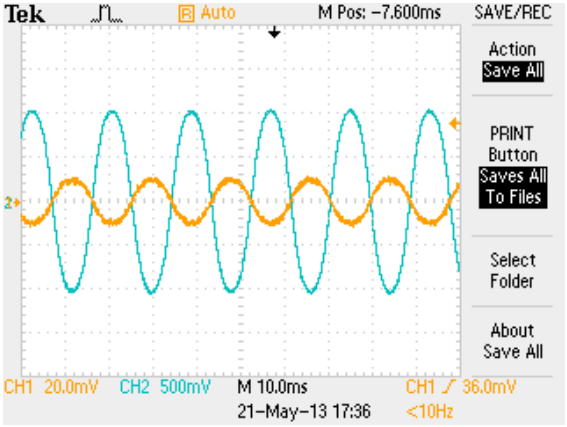

Figure 5.7: Voltage and current plot of the generator with 1 ohm load in phase A

Channel 1: Current in phase A

Channel 2: Voltage in phase A

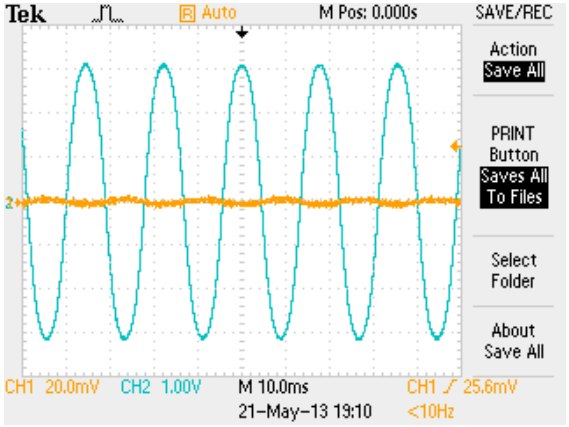

Figure 5.8: Voltage and current plot of the generator with 32 ohm (max) load in phase A

Channel 1: Current in phase A

Channel 2: Voltage in phase A

The generated voltage value shown in Figure 5.8 is higher because the machine is tested at a speed of 550 rpm whereas the simulation shows the result for the rated speed of 240 rpm. Naturally the hardware test results show higher value in agreement with Equation 8, Figure 5.8 and the back emf equation for a BLDC/PMSG given below (re-arranging equation 21):

$$e_{max} = N_m k_d k_p k_s B_g L R_{ro} N_{spp} n_s \omega_m \quad (25)$$

All of which prove that if speed increases, frequency increases and hence the magnitude of generated voltage is increased.

Figure 5.9 and 5.10 show the plot of rms voltage and current as calculated in equation 20 and 21 for a range of values in load resistance.

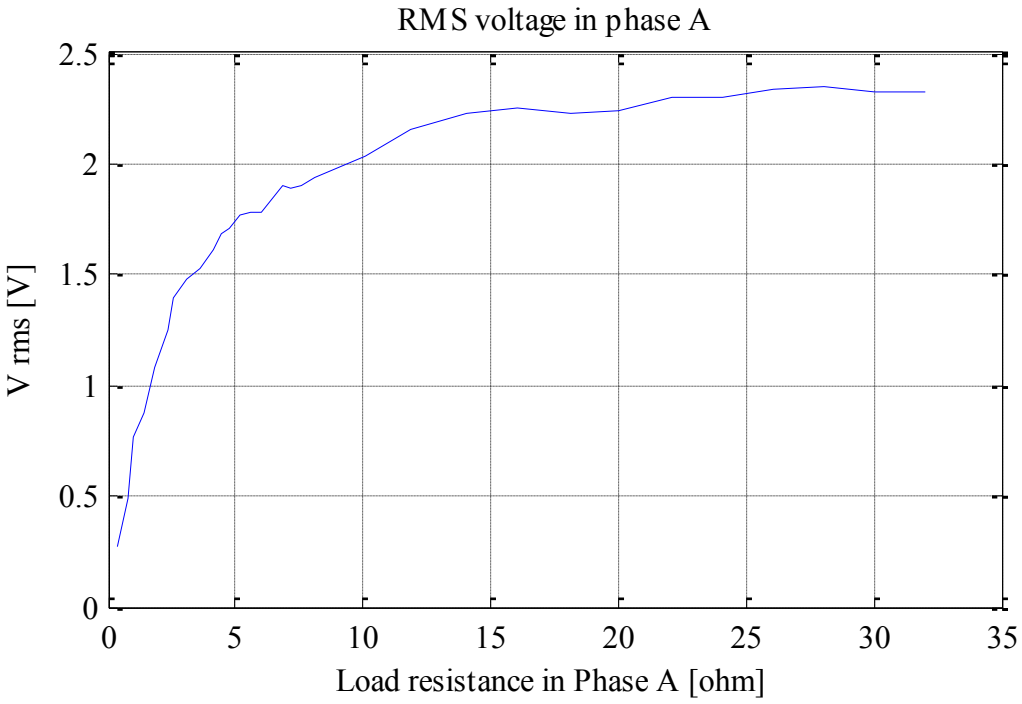

Figure 5.9: Voltage variation for load change in phase A

Figure 5.11 shows the power curve plot given by the product of V_{rms} & I_{rms} .

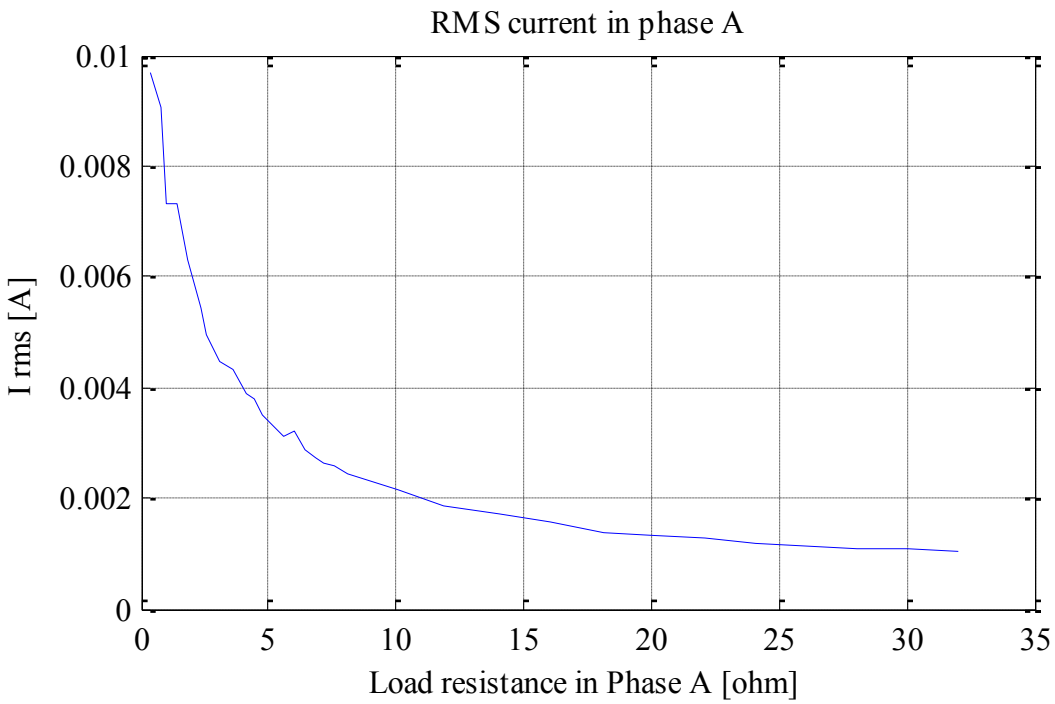

Figure 5.10: Current variation for load change in phase A

5.3. POWER CURVE PLOT

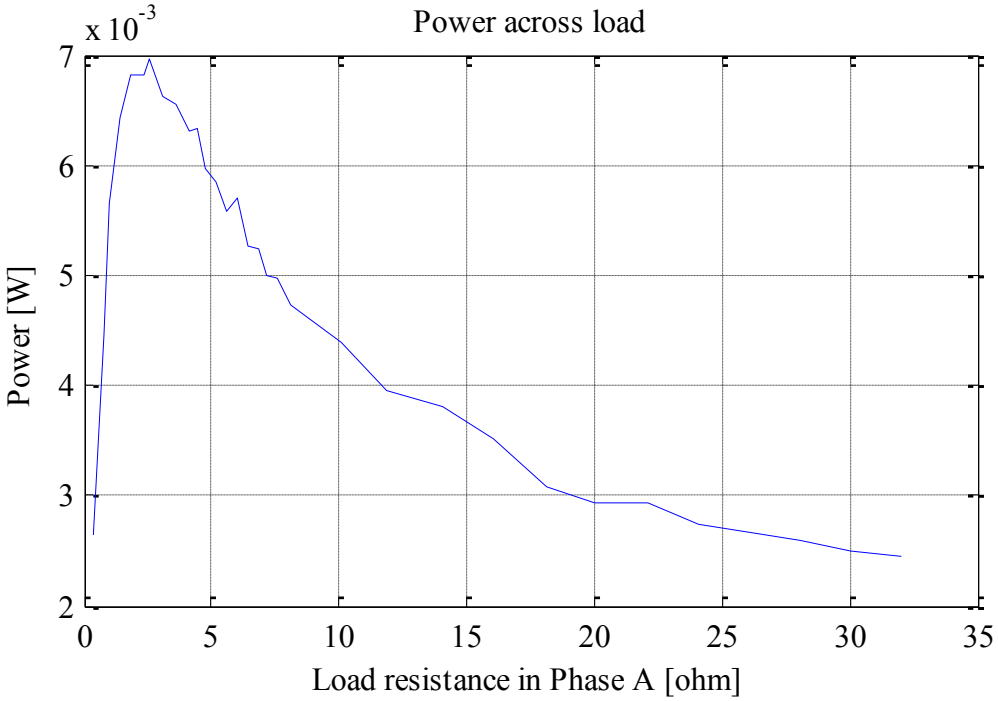

Figure 5.11: Power across load in phase A

Value of power in Figure 5.11 is calculated by the formula:

$$P_{rms} = V_{rms}.I_{rms} \tag{26}$$

A huge disturbance or non-uniform variation in power can be observed. This is due to the variation in speed of rotation of the DC motor used to rotate the PMSG. As discussed previously, there is no precise control over speed of the DC machine and the speed at measurement could be within a range of $\pm 2\%$ of 550 rpm.

Since the power curve is non-uniform and fine variation in load resistance is not possible since the variac has physical limitations, a curve fit may be achieved to obtain a clearer idea. But for accurate results of a quadratic type curve fit for a Weibull type data distribution (non-negative data points), the power values need to be plotted across conductance ‘G’ instead of resistance ‘R’.

6. CONCLUSION & FUTURE SCOPE

This thesis work describes how a PM generator can be built for a low speed hydrokinetic turbine. This helps in eliminating the gear systems which is often the weakest link in the whole turbine system and which is the cause to considerable loss of mechanical energy delivered through the shaft.

Hydrokinetic energy extraction particularly wave and tidal energy extraction systems, are in its initial years as far as scale of implementation is concerned. Their contribution to the total energy production of the country when compared to that by fossil fuels is less. Several hydrokinetic turbine structures have been briefly discussed and been compared to wind turbines and their basic functionality is found to be similar. Permanent Magnet Synchronous Generator is a good choice when compared to an Induction machine for low power applications like the one this generator is built for. Since it is rare or highly expensive to find a generator built for low speeds such as 240 rpm, this report lays the ground work to design and build a machine that can run at such low speeds.

Individual sections of the generator are separately designed and a new slot design is incorporated to keep the windings close to the magnets. This mildly compensates for the increased air gap taken in the machine to significantly reduce the cogging torque. The designed machine is simulated in RMXprt and Maxwell 2D to observe its electrical characteristics and the magnetostatic and transient behavior to watch for saturation. The design performs well on both fronts. The hardware was however was not exactly matched to the design specifications. Due to mechanical constraints seen after manufacturing like ill-considered filling factor value, shrunk outer diameter of the stator during design stage

and other minor deviations, only 30 turns were able to fit instead of 50 and hence the power produced does not completely agree with the simulation results but closely follows expected values. Since the machine is low power, it was seen that the resistance for 30 turn winding was 1.4 Ω largely restricting the load value that can be attached to its output side. Owing to this fact, a wide range of load resistances were attached and their performance was tested. The power curve was plotted to observe its behavior at various higher loads and it is seen the power produced is considerably low with the existing design and needs better optimized design and a larger structure to achieve higher power ranges.

The generator is tested for both open circuit and under load conditions. The power curve is plotted for a range of load values on a single phase and the results are presented.

The generator built in this project was to suit a compact and portable type turbine system that can be fitted about a marine locomotive or even a hydrokinetic turbine test bench of sorts for demonstration. The design procedure demonstrated in this article can be utilized to build bigger and higher power generators for large scale applications.

APPENDIX

The PMSG was designed using formulae from various text books and articles. The code was programmed into Matlab to obtain the design values. It is presented below. This code can be used to scale the machine as desired. This code hence can be treated as a plug and play program.

```
% % PMSG design for Hydrokinetic project; Guidance: Dr. J. W. Kimball.
% % By - Amshumaan R Kashyap.
%**********************************************************************
% % Mechanical dimensions
%**********************************************************************
****
% % P or Nm - No. of poles.
% % lambda - Tip speed ratio
% % Pitch angle = 12 deg fixed previously; now 8 to 8.5 deg is used
% % Cl - Lift co-efficient
% % Cd - Drag co-efficient
% % C - Cl/Cp
% % B - No. of blades
% % Cp - Power co-efficient; Max 0.395 at lambda = 5.2
% % Cpa & Cpb are just branches of Cp for simplification sake
% % r - Blade radius in inches converted to meters [m]
% % wm - (Mechanical) Rotational speed of the hydrokinetic turbine in
rad/s
% % v - Water velocity in m/s
% % rho - Water density in kg/m^3 at 25 deg C
% % theta_p - Angular pole pitch
% % D - Stator inner diameter [m] (Twice Rsi)
% % tP - Pole pitch
% % tC - Coil pitch (equal to tP in case of integral Nspp)
% % tS - Slot pitch
% % alpha_cp - Coil pitch in electrical radians = 1 for integral Nspp
% % L/tP ratio can be chosen from 0.6 to 0.7
% % L - Machine axial length [m]
% % Wbi - Back iron width [m]
% % Rso - Outer radius of stator [m]
% % Rsb - Stator back iron radius [m]
% % Rsi - Inside stator radius [m] = D/2
% % Rro - Outside rotor radius [m]
% % Rri - Rotor inside radius [m]; Also the rotor shaft radius.
% % lg - Length of air gap [m]
% % Nspp - No. of slots per pole per phase [integer or fraction is
allowed integral number is chosen to keep it full pitch.
% % Ns - No. of stator slots
% % Nst - No. of stator tooth = Ns
% % Nsp - No. of slots per phase
% % Nsm - No. of slots per magnet pole
% % Wtb - Tooth width [m]
```

```
% % Wsi - Slot width inside shoes [m]
% % Ws - Width of slot opening [m]
% % Wt - Tooth width at stator surface [m]
% % Wsb - Width of slot bottom [m]
% % Wxi - Width of extra iron (defined by amshu) [m]
% % theta_s - Angular slot pitch
% % theta_se - Slot pitch in electrical radians
% % alpha_sd - Slot depth fraction (4% to 5%)
% % d1 - lip height or pole shoe height (i'm calling it this way)[m]
% % d2 - wedge height [m]
% % d12 = d1 + d2 - just a way of denoting them [m]
% % hs - height of slot (OR ds - depth of slot) [m]
% % T - Mechanical torque
% % S - Arc length of magnet [m]
% % Se - Extra arc length considering 90% occupance of magnet on rotor
[m]
% % Rre - Extra rotor length added with previous rotor length 'Rro'[m]
% % theta_m - Sector angle of magnet [rad]
% % As - Area of the slot [mm^2]
%**************************************************************************
% % Wiring
%%*************************************************************************
% % kw - Stator winding factor; Assuming full pitch coil => kw = 0.955
% % dia - diameter of the AWG wire used
% % Ac - Total area of coil (for ns turns in the slot)
% % Jc - Current density of the slot/conductor [A/m^2]
% % Rs - Slot resistance
% % Re -  End turn resistance
% % Rph - Phase resistance
% % rho - Resistivity of copper wire [ohm.m]
%**************************************************************************
% % Magnetic and Electrical parameters
%**************************************************************************
% % N - Synchronous speed [rpm]
% % rps or wm - mechanical speed in rotations per second = N/60 or
rpm/60
% % wr - electrical rotor speed [rps]
% % f - Frequency of synchronous field in Hz -> 5 to 60 is feasible
range
% % Nph - No. of phases ( 3 phase generator)
% % Te - Electrical torque [Nm]
% % Fl - Frictional loss = 1% to 3% of rated output power [W]
% % Bav - Specific magnetic loading (Randomly chosen as 0.6 Tesla for
now)
% % Bmax - maximum steel flux density [Tesla] - Converted from Kilo
% % Pm - Output power of hydrokinetic turbine (Mechanical power)
% % kst - lamination stacking factor; 0.5 to 0.95 typical values ->
Hanselman's text book; 0.92 in Mittle & Mittal
% % phi or phi_g - Air gap flux per pole
% % Q - Output of alternator [VA]
% % pf - Power factor considered
% % Is - Peak slot current [A]
% % kd - Distribution factor
% % kp - Pitch factor (formula here is for non-sinusoidal or
trapezoidal back emf
```

```
% % ks - Skew factor = (1-(theta_se/(2*pi))) or
(sin(theta_se/2))/(theta_se/2)
% %      Based on square wave flux density or sinusoidal flux density
% % emax - Max emf generated with existing hardware specifications
% % emf - targeted back emf to be generated (Design approach)
% % Is - Total slot current when one phase is producing the desired
torque at once
% % Iph - Phase current when emf is a square wave and all phases are
conducting
%**************************************************************************
% % Magnet specifications (Magnet chosen from Apex magnets)
%**************************************************************************
% % Mod - Magnet Outer Diameter = 43 mm = 0.043 m
% % Mid - Magnet Inner Diameter = 39 mm = 0.039 m
% % lm - Magnet (axial) length = 5 mm = 0.005 m
% % AA - Arc Angle = 30 Degrees
% % Grade - N45H
% % Mir - Magnet Inner Radius
% % Mor - Magnet Outer Radius
%**************************************************************************
% % Diameters output
%**************************************************************************
% % Dso - Outermost diameter of generator or stator outer diameter
% % Dsi - Stator inside diameter (Enclosing the slots)
% % Dro - Rotor outer diameter (Enclosing magnets)
% % Dri - Rotor inner diameter or shaft dia
%**************************************************************************
% % Theoretical values
%**************************************************************************
% % Pm - mechanical power [watts]
% % Pe - electrical power [watts]
% % emf or Vdc - Back emf or the DC voltage output after the 3 phase
rectifier
% % Idc - DC current output after the 3 phase rectifier
% % Pcl - Core loss [W/lb] (Use Pcl/0.4535 to convert to W/kg)
% %       Value obtained from ARMCO industries datasheet on Protolam
% % Pr - Ohmic loss (sum from each phase)
% % Ps - Stray losses (Includes friction and windage losses and so on)
% % eff - efficiency in %ge
%**************************************************************************
%
% clear all
% clc
%
% N = 240;
% rps = N/60;                    % rps = rpm * (2pi/60)
% P = 12;
% wm = 2*pi*rps;                 % The lowest rpm turbine runs at
%
% f = P*N/120;
% Nm = P;
% wr = (P/2)*wm;                 % in rps
% Bav = 0.52;                    % Upto 100 KVA ??
% kst = 0.7;
%
% Bmax = 13.7e3/10000;           % [T] where 1 Tesla = 10,000 Gauss.
```

```
% lm = 5/1000;                     % 5 mm
% Mod = 43/1000;
% Mid = 39/1000;
%
% Mir = Mid/2;
% Mor = Mod/2;
% theta_p = 2*pi/Nm
% S = Mir*theta_p*180/pi;
% Se = 1.1 * S;
% Re = Se/(theta_p*180/pi);
% x = Mor - Mir;
% Rro = Re + (Mor - Mir);
% Dro = Rro * 2;
%
% lg = 0.004;                       % D is assumed 47mm implies air gap
is 2 mm wide
% % lg = 0.014*tP
% % lg = (3e-3)*(sqrt(P/2))*tP    % Pg 371 of Lipo
% D = (Dro + (2*lg));
% tP = pi*D/P;
% L = 25/1000;                      % Fixing length based on
% % L_tP = 0.7;                     % If I change 'L' manually, I must
change it here and make sure to calculate 'phi' & 'Wbi' accordingly
% % L = tP*L_tP;
%
% % This is to calculate 'L':
% % k_prime = 11*Bav*q*kw*1e-3;
% % pf = 0.8;
% % Q = Pout/(pf*1000)
% % L = Q/(k_prime*(D^2)*rps)
%
% Rsi = Rro + lg;
% % D = Rsi*2
% phi = Bav*(pi*D*L/P);             % Pg 505 of Mittle
% Wbi = phi/(2*Bmax*kst*L);         % Is Bav and Bmax same? Here Bmax is
to be used..
% Rri = Rro - lm - Wbi;
%
% Nph = 3;
% Nspp = 1;                         % Integral no. Implies tC = tP
% Ns = Nspp*Nm*Nph;
% Nsp = Ns/Nph;
% tC = tP;
% tS = pi*D/Ns;
% Nsm = Nspp*Nph;                   % Or Ns/Nm
% Nst = Ns;
%
% Wtb = 2*Wbi/Nsm;                  % Cross check with formula on pg 507
of Mittle
% Ws = ((tS - Wtb)/(5/3));          % Because of the new type of slot
design, make sure Ws is greater than Wtb.
% Wsb = Wtb;                        % Only because of the new type of
slot design - What I have chosen.
% theta_s = tS/Rsi;
% % theta_s = (2*pi)/Ns;            % Other way of calculating; both
yield same values
```

```
% alpha_sd = 0.4;                  % assumption as observed in Mittle
% d12 = alpha_sd*Wsb;
% Wsi = (((Rsi+d12)*theta_s)-Wtb);
% Wt = Wtb +((2/3)*Wsi);           % My assumption that 2/3rd of slot
opening is covered by teeth
%
% ds = 10*d12;                     % assuming d12 is 10% of total slot
height
% hs = ds;
% Rsb = Rsi + hs;
% Rso = Rsb + Wbi;
% Wxi = (Rsb*theta_s)-Wsb;
% Rr = Rsi - lg;                   % Or (Rsb - ds - lg)
% As = 0.5*(Wsb+Wxi)*hs;           % m^2
%
% alpha_cp = tC/tP;                % Should be one since integral Nspp
%
% % Conductors per slot I have chosen to be 45; Hence calculations
below are hashed for now
% % theta_se = pi/Nsm
% % kd =(sin(Nspp*theta_se/2))/(Nspp*sin(theta_se/2));
% % kp = alpha_cp;                 % Will just result in '1'
% % ks =1;                         % ks = 1 - (theta_se/(2*pi)) but
since I do not need skewing for now, 1 is chosen
% % Is = T/(Nm*kd*kp*ks*Bav*L*Rro*Nspp)     % 'Bg' is to be used here
not 'Bav'
% % Iph =
%
% P_f_Nspp_Ns = [P f Nspp Ns]
% tP_tC_in_mm= [tP tC]*1000
% L_Wbi_Wxi_Wtb_Wt_Ws_Wsi_d12_ds_in_mm = [L Wbi Wxi Wtb Wt Ws Wsi d12
ds]*1000
% Rso_Rsi_Rro_RRi_lg_in_meters = [Rso Rsi Rr Rri lg]
% Rso_Rsi_Rro_RRi_lg_in_mm = [Rso Rsi Rro Rri lg]*1000
% Diameters_Dso_Dsi_Dro_Dri_in_mm = [Rso Rsi Rro Rri]*2*1000
%
% % Mechanical Power output
% T = 0.08;                    % Obtained from mech team in Nm
% Pm = T*N*2*pi/60
%
% % Output from the existing hardware
% theta_se = pi/Nsm;
% kd = (sin(Nspp*theta_se/2))/(Nspp*sin(theta_se/2));
% kp = alpha_cp;               % Also kp = theta_ce/pi
% ks = 1;                      % since the magnets are not skewed
% Bg = Bav;                    % Since already tis was considered for
design
%                              % formula in pg 69 Hanselmann
% ns = 30;
% emax = Nm*kd*kp*ks*Bg*L*Rro*Nspp*ns*wm;
% Is = T/(Nm*kd*kp*ks*Bg*L*Rro*Nspp);
% i = T*wm/emax;
% Is2 = ns*i;
% Iph = Is/(Nph*ns);
% dia = 0.54*1e-3;             % [m]
% Ac = (pi*(dia^2)/4)*ns;      % [m^2]
```

```
% kcp = Ac/As
% Jc = Is/(kcp*As);           % [A/m^2] (range is 4 to 10 MA/m^2
% rho = 1.68e-8;              % [ohm.m]@ 20 deg C
% Rs = (rho*(ns^2)*L)/(kcp*As);
% Re = (rho*(ns^2)*pi*tC)/(2*kcp*As);
% Rph = Nsp*(Rs+Re);
% emax_Is_Iph_Rph = [emax Is Iph Rph]
% Pcl = 0.804 /0.4535;        % to convert from lb to kg [W]
% Pr = Nph*(Iph^2)*Rph       % [W]
% Pg = emax*Iph
% % Ps = ;                    % stray losses neglected
% eff = (Pm/(Pm+Pr+Pcl))*100
```

BIBLIOGRAPHY

[1] British_Petroleum, "BP Statistical Review of World Energy June 2012," 2012, pp. 1 - 48.

[2] R. Gelman, "2010 renewable Energy Data Book," Scott Gossett, Ed.: US Department of Energy, 2010, pp. 136.

[3] A. McCrone, "Global Trends in Renewable Energy Investment - 2012," Frankfurt School of Finance & Management, 24 July 2012, pp. 82.

[4] Rathor, "Energy Statistics 2012 - Govt. of India." Central Statistics Office, April 2013, pp. 99.

[5] S. Benelghali, M. E. H. Benbouzid, and J. F. Charpentier, "Comparison of PMSG and DFIG for Marine Current Turbine Applications," presented at XIX International Conference on Electrical Machines - ICEM, October 2010.

[6] H. Li and Z. Chen, "Overview of different wind generator systems and their comparisons," *IET Renewable Power Generation*, vol. 2, pp. 123 - 138.

[7] R. Parekh, "AC Induction Motor Fundamentals," in *AN887*: MicrochipTechnology, December 2003, pp. 1 - 24.

[8] X. J. Yao, S. Liu, X. D. Wang, C. c. Guo, Z. X. Xing, and H. L. Jiang, "Doubly-Fed Induction Generator Control for Variable-Speed Wind Power Generation System," presented at International Conference on Mechatronics and Automation, August 2009.

[9] X. Yang, J. Hudgins, and D. Patterson, "Permanent magnet generator design and control for large wind turbines " presented at Power Electronics and Machines in Wind Applications (PEMWA), July 2012.

[10] Y.-S. Xue, L. Han, H. Li, and L.-D. Xie, "Optimal Design and Comparison of Different PM Synchronous Generator Systems for Wind Turbines," presented at International Conference on Electrical MAchines and Systems - ICEMS, jan 2009.

[11] G. Kömürgöz and T. Gündoğdu, "Comparison of salient pole and Permanent Magnet Synchronous Machines designed for wind turbines " presented at Power Electronics and Machines in Wind Applications (PEMWA), July 2012.

[12] J. Tamura, "Calculation Method of Losses and Efficiency of Wind Generators," in *Wind Energy Conversion Systems - Technology and Trends*, S M Muyeen, Ed.: Springer publications, 2012, pp. 25 - 51.

[13] J. C. M. Vieira, A. Morelato, L. C. P. Da_Silva, V. F. Da_Costa, and F. A. B. Lemos, "Comparative Analysis between Synchronous and Induction Machines for Distributed Generation Applications " *IEEE Transcations on Power Systems*, vol. 21, pp. 301 - 311.

[14] U.S Department of Energy, "The Inside of a Wind Turbine," accessed on, http://www1.eere.energy.gov/wind/inside_a_wind_turbine.html.

[15] M. S. Güney and K. Kaygusuz, "Hydrokinetic energy conversion systems: A technology status review," *Renewable and Sustainable Energy Reviews*, vol. 14, pp. 2996-3004.

[16] P. Jacobson, "Assessment and Mapping of the Riverine Hydrokinetic Energy Resource in the Continental United States," Electric Power Research Insitute (EPRI), Dec 2012.

[17] "Electric Power Annual 2011," U.S. Energy Information Administration, Jan 2013.

[18] M. Simmons and L. Guey-Lee, "Renewable Energy Trends in Consumption and Electricity 2008," U.S. Energy Information Administration, Washington, DC, August 2010.

[19] Department of Energy, "LIST OF COMPREHENSIVE PLANS April 2013," April 2013.

[20] "Memorandum of Understanding Between the FERC and the California Natural Resources Agency, California Enviromentl Protection Agency and the California Public Utilities Commission," 2010.

[21] "Marine & Hydrokinetic Projects, Industries," 2013.

[22] "Wind Energy Background," accessed on, http://www.dolcera.com/wiki/index.php?title=Wind_Energy_Background.

[23] H. Li, G. A. Taylor, A. M. Abutunis, K. Chandrashekhara, A. R. Kashyap, and J. W. Kimball, "DESIGN AND PERFORMANCE EVALUATION OF A HYDROKINETIC COMPOSITE TURBINE SYSTEM," presented at Society for the Advancement of Material and Process Engineering, 2013.

[24] "Marine energy more than just a drop in the ocean," accessed on, http://www.lunarenergy.co.uk/.

[25] S. E. Ben Elghali, M. E. H. Benbouzid, and J. F. Charpentier, "Marine Tidal Current Electric Power Generation Technology: State of the Art and Current Status," in *Proc. Electric Machines & Drives Conference, 2007. IEMDC '07. IEEE International*, 2007, vol. 2, pp. 1407-1412, 10.1109/iemdc.2007.383635.

[26] C. Lang, "Harnessing tidal energy takes new turn " *IEEE Spectrum* vol. 40, pp. 13.

[27] G. Lampman and R. Smith, "ROOSEVELT ISLAND TIDAL ENERGY (RITE) ENVIRONMENTAL ASSESSMENT PROJECT," Albany, NY.

[28] Free Flow Power, "Mississippi River Projects " accessed on, http://free-flow-power.com/projects/mississippi_river_projects.

[29] A. M. Ragheb and M. Ragheb, "Wind Turbine Gearbox Technologies," presented at Proceedings of the 1st International Nuclear and Renewable Energy Conference, 2011.

[30] J. McGuinn, "Wind Turbines: Clean Energy, but Energy-Efficient?," in *Gear Technology*, 2011.

[31] W. Musial, S. Butterfield, and B. McNiff, "Improving Wind Turbine Gearbox Reliability," presented at 2007 European Wind Energy Conference, May 2007.

[32] Windpower Engineering & Development, "Why gearboxes fail and a solution to lower drivetrain costs," accessed on, http://www.windpowerengineering.com/maintenance/why-gearboxes-fail-and-a-solution-to-lower-drivetrain-costs/.

[33] R. Errichello and J. Muller, "Gearbox Reliability Collaborative Gearbox 1 Failure Analysis Report." Oak Ridge, TN: National Renewable Energy Laboratory, Dec 2010 - Jan 2011.

[34] R. Takahashi, H. Ichita, J. Tamura, M. Kimura, M. Ichinose, M.-o. Futami, and K. Ide, "Efficiency calculation of wind turbine generation system with doubly-fed induction generator," presented at XIX International Conference Electrical Machines (ICEM), Sept 2010.

[35] D. Borkowski and T. Wegiel, "Small Hydropower Plant With Integrated Turbine-Generators Working at Variable Speed," *IEEE Transactions On Energy Conversion*, pp. 1 - 8.

[36] H. Li and Z. Chen, "Optimal direct-drive permanent magnet wind generator systems for different rated wind speeds " presented at 2007 European Conference on Power Electronics and Applications, 2007.

[37] H. Polinder, F. F. A. v. d. Pijl, G. J. d. Vilder, and P. J. Tavner, "Comparison of Direct-Drive and Geared Generator Concepts for Wind Turbines," *IEEE Transactions On Energy Conversion*, vol. 21, pp. 725 - 733.

[38] "Alnico Magnet Properties," Dexter Magnetic Technologies Inc., Ed., 2010.

[39] "Nd-Fe-B magnet properties," Dexter Magnetic Technologies Inc.. Ed., 2010.

[40] "Sm-Co magnet properties," Dexter Magnetic Technologies inc.. Ed., 2010.

[41] S. R. Trout, "Rare Earth Magnet Industry in the USA: Current Status and Future Trends," presented at XVII rare Earth Magnet Workshop, 2002.

[42] H. Oman and R. Simpson-Clark, "Permanent magnets for vehicle-propulsion motors: cost/availability," in *Proc. Energy Conversion Engineering Conference, 1996. IECEC 96., Proceedings of the 31st Intersociety*, 1996, vol. 1, pp. 91-96 vol.1, 10.1109/iecec.1996.552851.

[43] I. Petrov and J. Pyrhonen, "Performance of Low-Cost Permanent Magnet Material in PM Synchronous Machines," *Industrial Electronics, IEEE Transactions on*, vol. 60, pp. 2131-2138.

[44] H. G. C, L. Jinfang, G. Alexander, and M. Melania, "Current Status of Rare-Earth Permanent Magnet Research in USA," *International Journal of Iron and Steel Reserach* pp. 1- 10, 12/22/2013.

[45] W. Fengxiang, B. Jianlong, H. Qingming, and P. Jian, "Design features of low speed permanent magnet generator direct driven by wind turbine " in *Proc. Proceedings of the Eighth International Conference on Electrical Machines and Systems, 2005. (ICEMS 2005)*, 2005, 10.1109/ICEMS.2005.202699.

[46] V. N. Mittle and A. Mittal, *Design of Electrical Machines*, fifth ed. Delhi: M K Offset Printers, 2009.

[47] B. J. Chalmers, W. Wu, and E. Spooner, "An axial-flux permanent-magnet generator for a gearless wind energy system " presented at Proceedings of the 1996 International Conference on Power Electronics, Drives and Energy Systems for Industrial Growth, 1996.

[48] J.-Y. Choi, S.-M. Jang, and B.-M. Song, "Design of a Direct-Coupled Radial-Flux Permanent Magnet Generator for Wind Turbines," presented at 2010 IEEE Power and Energy Society General Meeting, 2010.

[49] J. F. Gieras, *Permanent Magnet Motor Technology (Design and Applications)*, 3rd ed. Florida: CRC Press, 2010.

[50] D. C. Hanselman, *Brushless Permanent Magnet Motor Design*. USA: McGraw-Hill, 1994.

[51] T. Liu, S. Huang, Q. i. Deng, Q. Pu, and K. Huang, "Effect of the Number of Slots per Pole on Performance of Permanent Magnet Generator Direct-Driven by Wind Turbine," presented at 2011 International Conference on Electrical Machines and Systems (ICEMS), 2011.

[52] Y.-K. Lin, Y.-N. Hu, T.-K. Lin, H.-N. Lin, Y.-H. Chang, C.-Y. Chen, S.-J. Wang, and T.-F. Ying, "A method to reduce the cogging torque of spindle motors," *Journal of Magnetism and Magnetic Materials*, pp. 180 - 182.

[53] "Silicon Steel (Electrical Steel)," accessed on, http://www.protolam.com/page7.html.

[54] H. A. Toliyat and G. B. Kliman, "Synchronous Motor Analysis and Design," in *Handbook of Electric Motors*, Second ed, 2004.

[55] J. R. J. Hendershot and T. J. T. J. E. Miller, *Design of Brushless Permanent Magnet Motors*: Magna Physics Publishing, 1994.

[56] M. Liwschitz-Garik and C. C. Whipple, *Electric machinery*: D. Van Nostrand company, inc., 1947.

[57] "Installation and Operating Manual," in *Integral Horse Power DC Motor - CD5318*: Baldor Electric, 2009, pp. 1 - 30.

VITA

Amshumaan R Kashyap received his Bachelor of Engineering degree in Electrical & Electronics Engineering in 2011 from Visveswaraya Technological University. He then received his Masters of Science degree in Electrical Engineering from Missouri University of Science and Technology in May 2013. His research interests include Electric motors & drives linked to renewable energy and DC – DC power electronic converters.